Control of 3' splice site selection by the yeast splicing factor Fyv6

Katherine A. Senn[1]*, Karli A. Lipinski[2]*, Natalie J. Zeps[1], Amory F. Griffin[1],

Max E. Wilkinson[3, 4], Aaron A. Hoskins[1,2]

*indicates co-first authors

[1] Department of Biochemistry, University of Wisconsin-Madison, Madison, WI 53706 USA

[2] Department of Chemistry, University of Wisconsin-Madison, Madison, WI 53706 USA

[3] MRC Laboratory of Molecular Biology, Cambridge CB2 0QH UK

[4]Present Addresses: Broad Institute of MIT and Harvard, Cambridge MA 02142 USA and McGovern Institute for Brain Research, Massachusetts Institute of Technology, Cambridge, MA 02139 USA

CORRESPONDING AUTHORS:

Aaron A. Hoskins, ahoskins@wisc.edu

Max E. Wilkinson, mwilkin@mit.edu

RUNNING TITLE: Structure and Function of the Splicing Factor Fyv6

KEYWORDS: yeast, spliceosome, pre-mRNA splicing, cryo-EM, snRNA, snRNP, structure, RNA-Seq

ABSTRACT

Pre-mRNA splicing is catalyzed in two steps: 5' splice site (SS) cleavage and exon ligation. A number of proteins transiently associate with spliceosomes to specifically impact these steps (1st and 2nd step factors). We recently identified Fyv6 (FAM192A in humans) as a 2nd step factor in *S. cerevisiae*; however, we did not determine how widespread Fyv6's impact is on the transcriptome. To answer this question, we have used RNA-seq to analyze changes in splicing. These results show that loss of Fyv6 results in activation of non-consensus, branch point (BP) proximal 3' SS transcriptome-wide. To identify the molecular basis of these observations, we determined a high-resolution cryo-EM structure of a yeast product complex spliceosome containing Fyv6 at 2.3 Å. The structure reveals that Fyv6 is the only 2nd step factor that contacts the Prp22 ATPase and that Fyv6 binding is mutually exclusive with that of the 1st step factor Yju2. We then use this structure to dissect Fyv6 functional domains and interpret results of a genetic screen for *fyv6Δ* suppressor mutations. The combined transcriptomic, structural, and genetic studies allow us to propose a model in which Yju2/Fyv6 exchange facilitates exon ligation and Fyv6 promotes usage of consensus, BP distal 3' SS.

INTRODUCTION

Precursor messenger RNA (pre-mRNA) splicing is catalyzed by a large macromolecular complex called the spliceosome. Spliceosomes are composed of 5 small nuclear ribonucleoproteins (snRNPs), each composed of a small nuclear RNA (snRNA; U1, U2, U4, U5, and U6) and several different protein splicing factors. The snRNPs and dozens of other proteins assemble *de novo* at each intron to form spliceosomes. Spliceosomes are highly dynamic and form different complexes as proteins and snRNAs join and leave. Many of these complexes have been characterized biochemically, genetically, and by cryo-electron microscopy (cryo-EM) (Plaschka et al., 2019). The splicing reaction itself is carried out in two sequential transesterification reactions (**Fig. 1A**). First, the 5' splice site (5' SS) is cleaved during formation of an intron lariat (1st step). Second, the intron lariat is removed simultaneously with exon ligation at the 3' SS (2nd step).

The integrity of the genetic information contained within a pre-mRNA depends on correct identification of the 5' and 3' SS by the splicing machinery since a single nucleotide shift in either site could destroy a protein reading frame. In yeast, several DExD/H-box ATPases function to limit usage of suboptimal SS by enhancing splicing fidelity (Chung et al., 2023; Semlow and Staley, 2012). Two of these ATPases, Prp16 and Prp22, impact the fidelity of the 1st and 2nd catalytic steps, respectively. In addition to these roles, Prp16 is also required for remodeling of the spliceosome to permit the 1st-to-2nd step transition (Schwer and Guthrie, 1992), and Prp22 is essential for releasing the mRNA product (Company et al., 1991). While Prp16 does not need to be present during the 1st step (Chung et al., 2023), Prp22 is required to be present for exon ligation if the branch point (BP) to 3' SS distance is $\geq$ 21 nucleotides (nt) (Schwer and Gross, 1998). Despite many biochemical, single molecule, and structural studies, how spliceosomes promote usage of BP distal, Prp22-dependent 3' SS has remained elusive.

Identification of the correct 3' SS is an especially challenging problem given that the consensus sequence in *Saccharomyces cerevisiae* (yeast) and humans is just three nucleotides

62 (YAG, Y=U or C). Cryo-EM structures of spliceosome product (P) complexes have revealed how
63 these nucleotides can be recognized within the spliceosome active site (Bai et al., 2017; Fica et
64 al., 2019; Liu et al., 2017; Wilkinson et al., 2017; Zhang et al., 2019). The AG 3' SS dinucleotide
65 is recognized by formation of non-Watson Crick base-pairing interactions with the 5' SS +1G and
66 BP adenosine, while the pyrimidine at the -3 position of the 3' SS is recognized by the Prp8
67 protein. Given this short consensus sequence, multiple different splicing factors also help to
68 ensure that the correct 3' SS is utilized, including Cwc21 and the 2nd step factors Slu7, Prp18, and
69 Prp22 (Crotti et al., 2007; Frank and Guthrie, 1992; Gautam et al., 2015; Kawashima et al., 2014;
70 Roy et al., 2023; Semlow et al., 2016). It is believed that Slu7 and Prp18 help to stabilize 3' SS
71 docking to the active site and that this contributes to 2nd step efficiency. It has been proposed that
72 Prp22 antagonizes 3' SS docking to permit sampling of different 3' SS to ensure that optimal
73 sequences are used as a proofreading mechanism (Mayas et al., 2006; Semlow et al., 2016).
74 Importantly, identification of the correct 3' SS depends not just on identification of the YAG
75 sequence but also involves choosing which YAG sequence to use. Prp18 appears to aid in
76 selection of BP distal 3' SS and avoidance of BP proximal (and often non-consensus) 3' SS. This
77 observation could be due to Prp18 imposing a BP to 3' SS distance constraint, enforcing use of
78 canonical YAG 3' SS sequences, or a combination of the two activities.

79 Recently, Fyv6 was identified as a novel 2nd step factor in yeast (Lipinski et al., 2023).
80 Fyv6 is a homolog of the human protein FAM192A, which was identified in pre-C* structures of
81 the human spliceosome (Zhan et al., 2022). While the impact of FAM192A on human spliceosome
82 activity has not yet been well-characterized, loss of Fyv6 in yeast decreases 2nd step splicing
83 efficiency *in vitro* and results in use of an alternative 3' SS in the *SUS1* pre-mRNA *in vivo*. It is
84 likely that unassigned cryo-EM densities in yeast C* (just prior to exon ligation) and P complexes
85 correspond to Fyv6 since these densities are in analogous locations to that for FAM192A in the
86 human pre-C* structure (Zhan et al., 2022). However, the resolutions of the yeast C* and P

87 complex structures make unambiguous assignment of Fyv6 amino acid side chains and
88 interactions difficult.

89 Here, we use a combination of transcriptomic, structural, biochemical, and genetic assays
90 to elucidate how Fyv6 controls 3' SS usage in yeast. RNA-seq analysis reveals widespread
91 activation of alternative, BP proximal nonconsensus 3' SS in the absence of Fyv6 consistent with
92 biochemical assays that show Fyv6 facilitates splicing of 3' SS located $\geq$ 21 nt from the BP. To
93 further elucidate Fyv6 function, we determined a 2.3 Å cryo-EM structure of the yeast P complex
94 spliceosome in which Fyv6 can be modeled. The structure reveals interactions between Fyv6 and
95 Prp22 as well as a domain in Syf1 that interacts with either Fyv6 or the 1st step factor Yju2. 3D
96 classification allowed us to identify two additional conformational states of P complex and
97 provides insights into the coupling of 3' SS active site docking and the presence of 2nd step factors.
98 We then used this structural data to dissect the functional domains of Fyv6, interpret the results
99 of a genetic screen for suppressors of *fyv6Δ*, and to probe Fyv6 and Prp22 interactions.
100 Combined, we propose a model in which Fyv6 is recruited to the spliceosome via interactions with
101 the NTC component Syf1 in order to promote usage of BP distal, and Prp22-dependent, 3' SS.

102 **RESULTS**

103 **Deletion of *FYV6* Results in Widespread Use of Alternative 3′ Splice Sites**

104 Our previous work showed that loss of *FYV6* causes changes in 3' SS usage in the *SUS1*
105 pre-mRNA. To probe for changes transcriptome-wide, we used nonsense mediated decay (NMD)-
106 deficient (*upf1Δ*, WT) yeast cells expressing or lacking Fyv6. By suppressing NMD, we hoped to
107 limit degradation of alternatively spliced mRNA isoforms generated in the absence of Fyv6
108 (Sayani et al., 2008). Consistent with results from *fyv6Δ* strains, the *fyv6Δ upf1Δ* double mutant
109 strain also showed reduced growth at 30°C and cold-sensitive (*cs*) and temperature-sensitive (*ts*)
110 phenotypes relative to a *upf1Δ* control strain (**Fig. 1B**). We then used RNA-Seq to analyze the
111 isolated RNAs from these strains. As expected, many more changes in splicing were observed in

112 the *fyv6Δ upf1Δ* strain relative to the *fyv6Δ* strain (**Supplemental Fig. S1A, B; Supplemental**
113 **Tables S1, S2**). This is consistent with many mRNA isoforms generated due to loss of Fyv6 being
114 substrates for NMD. Loss of Fyv6 resulted in a number of changes in gene expression with many
115 non-intron containing genes also being up- or down-regulated (**Supplemental Fig. S1C**).

116 We compared and classified changes in splicing between strains containing or lacking
117 *FYV6* under permissive growth conditions (30°C) or after the yeast had been shifted to a non-
118 permissive temperature (16 or 37°C) for 1 h (**Fig. 1C**). In this case, we only considered events
119 resulting in at least a 10% change in the percent spliced in (PSI) value when *FYV6* is deleted. At
120 all temperatures, we see changes in alternative 3' SS usage in the *fyv6Δ* strain relative to the
121 *FYV6* background. For example, we detected use of the alternative 3' SS in the first intron of the
122 *SUS1* transcript as we previously reported (**Supplemental Fig. S1D**; Lipinski et al., 2023). We
123 also saw increased use of a cryptic, nonconsensus GAG 3' SS in the first, but not second, intron
124 of the *YOS1* transcript in the *fyv6Δ* data sets and confirmed this result by RT-PCR (**Supplemental**
125 **Fig. S1E, F**). We observed several cases of alternative 5' SS. However, the majority of these
126 alternative 5' SS were used with equal efficiencies in the WT and *fyv6Δ* strains (**Supplemental**
127 **Fig. S1G**).

128 The strains temperature shifted to 16°C had the largest number of changes due to *FYV6*
129 deletion and the strains shifted to 37°C the least. The temperature shift to 16° caused an increase
130 in the numbers of both alternative 3' SS and retained intron events detected (**Fig. 1C**). The
131 changes in alternative 3' SS used at each temperature were mostly unique with few events
132 detected under all three conditions (**Fig. 1D**). Collectively, we observed that 61 different RNAs
133 changed splicing patterns due to loss of Fyv6. For many of these mRNAs, we detected multiple
134 different 3' SS being used.

135 To investigate these splicing events more closely, we analyzed changes in usage of
136 alterative splice junctions by calculating the Fraction of Annotated Splicing (FAnS) in the presence

137 and absence of Fyv6 (Roy et al., 2023). FAnS ratios report the relative abundance of an alternative
138 splicing event in relation to the main spliced isoform. We calculated FAnS values for all exon
139 junction reads corresponding to usage of a canonical 5' SS and an alternative 3' SS for WT and
140 *fyv6Δ* strains at each temperature. We then calculated the ratios of the *fyv6Δ*/WT FAnS values
141 for each transcript. These results confirm changes in alternative 3' SS usage for both ribosomal
142 protein gene (RPG) and non-RPG transcripts at all conditions (**Fig. 1E**). We could not detect any
143 significant differences between RPG and non-RPG splicing with this analysis, suggesting that
144 differences in gene expression and splicing efficiencies between these two classes are not
145 correlated with alternative 3' SS usage. Combined these results show that Fyv6 plays a critical
146 role in defining mRNA isoform production in yeast, particularly under non-optimal growth
147 conditions such as temperature stress.

148 **Fyv6 Facilitates Usage of Branch Point Distal 3′ Splice Sites**

149 We next analyzed the features of the 3' SS impacted by Fyv6 loss. We used RNAs
150 collected from yeast grown at 30°C and sequenced the libraries at higher depth than those used
151 for the temperature-shift experiment described in **Fig. 1** (~400 million vs. 200 million reads;
152 **Supplemental Table S2**). We first identified alternative 3' SS used in each strain, annotated each
153 as being upstream (5') or downstream (3') of the canonical 3' SS (Grate and Ares, 2002), and
154 then calculated the FAnS ratio for each site. This analysis shows that the majority of the alternative
155 3' SS arising from Fyv6 deletion are upstream (**Fig. 2A**, pink points above the diagonal). When
156 these alternative 3' SS are mapped according to their nucleotide distance from the canonical site,
157 most of these are found within ~40 nt upstream (**Fig. 2B**, purple violin). Plotting these alternative
158 3' SS sites relative to their distance from the annotated BP reveals that the highest density of sites
159 is $\leq$ 20 nt from the BP for transcripts with the highest FAnS ratios (**Fig. 2C**, purple violin). It is
160 important to note that we did not map BP in Fyv6 deletion strains, and it is possible that in some
161 cases a shift in 3' SS usage could also coincide with a shift in the BP. Indeed, a small number of
162 alternative 3' SS detected in the Fyv6 data sets are located upstream of the annotated BP,

163 suggesting activation of an alternative BP and 3' SS. However, we believe that the changes are
164 predominantly due to usage of alternative 3' SS located between the annotated BP and canonical
165 3' SS.

166 The above results suggest that Fyv6 is important for splicing of 3' SS located distant from
167 the BP. To test this directly and systematically, we created a series of ACT1-CUP1 reporters with
168 various BP to 3' SS distances (9-50 nt, **Fig. 2D**, **Supplemental Table S3**) based on sequences
169 used in previous studies of 3' SS selection (Brys and Schwer, 1996; Frank and Guthrie, 1992;
170 Schwer and Gross, 1998). We transformed strains containing or lacking Fyv6 and without
171 debranchase (Dbr1) to limit degradation of lariat intermediates. We then detected RNA products
172 by primer extension and calculated the 2nd step (exon ligation) efficiency for each reporter (**Fig.
173 2E, F**). While loss of Fyv6 has minimal impact on exon ligation when BP to 3' SS distances are
174 short (9-15 nt), exon ligation efficiency decreases significantly at distances of 21 nt or greater. In
175 addition, we do not see evidence of cryptic BP usage in these assays. This result is consistent
176 with the RNA-seq analysis and supports a function for Fyv6 in facilitating splicing at BP distal 3'
177 SS.

178 Finally, we analyzed the sequence features of the alternative 3' SS activated by loss of
179 Fyv6 (**Fig. 2G, H**). For sites located upstream of the canonical 3' SS, we observed much greater
180 sequence variability relative to the canonical site. We detected increased use of highly variable 3'
181 SS including those with atypical HAU (H=A,C,U) and BG (B=C,U,G) motifs and confirmed
182 generation of new RNA isoforms for several of these by RT-PCR (**Fig. 2H, Supplemental Fig.
183 S2**). Increased use of variable 3' SS was also observed when the 2nd step factor *PRP18* was
184 deleted (Roy et al., 2023). However, the subset of RNAs most impacted by splicing factor deletion
185 appear to be different. For example, we were not able to detect changes in 3' SS usage for the
186 *UBC12*, *MAF1*, *MUD1*, *PHO85*, *SPT14*, or *YCL002C* transcripts in the *fyv6*Δ data sets as was
187 reported for *prp18*Δ (not shown). Prp18 and Fyv6 likely have transcript-specific effects on splicing

188 outcomes. Combined our results strongly support Fyv6 as a 2nd step splicing factor that facilitates
189 usage of consensus sites located distal to the BP *in vivo*.

190 **A High-Resolution Spliceosome Structure Reveals Fyv6 Interactions**

191 Previous structures of the yeast P-complex spliceosome were solved with resolutions at
192 the core ranging from 3.3 Å to 3.7 Å (Bai et al., 2017; Liu et al., 2017; Wilkinson et al., 2017), and
193 with peripheral components such as the Prp22 helicase, U2 snRNP, and Prp19 Complex (NTC)
194 at much lower resolutions (5-10 Å) that precluded detailed investigation. To improve the
195 resolution, we purified P complex as previously described by stalling spliceosome disassembly
196 with a dominant negative mutant of Prp22 (S635A) defective in mRNA release (Schwer and
197 Meszaros, 2000; Wilkinson et al., 2017). However, by collecting a much larger cryo-EM dataset
198 on a more modern electron detector, we were able to resolve the structure to 2.3 Å within the
199 catalytic core, as well as visualize peripheral components at resolutions from 3.0 Å – 3.7 Å (**Fig.
200 3A, B; Supplemental Fig. S3-S6; Supplemental Table S4**). This is the highest resolution
201 spliceosome structure to date. The high-quality density at the active site shows the positions of
202 bases unambiguously, confirming the manner of the non-Watson-Crick base pairing that mediates
203 3' SS recognition (Liu et al., 2017; Wilkinson et al., 2017). Monovalent ions bound at the active
204 site were previously shown to be important during the 1st step of splicing (Wilkinson et al., 2021),
205 and our data indicate that the positions of these ions are preserved after exon ligation. Additionally,
206 the density also shows a metal ion, likely potassium, that bridges the base pair between +1G of
207 the 5' SS and -1G of the 3' SS (**Fig. 3C**).

208 The 2nd-step splicing factor Prp22 is resolved at 3.0 Å resolution, allowing atomic
209 interpretation for the first time (**Fig. 3B** and later figures). Bases 13 – 21 of the 3' exon are visible
210 between the two RecA domains of Prp22 consistent with biochemical footprinting data (Schwer,
211 2008). The S635A mutation used to stall P complex is also visible; however, the origin of defective
212 mRNA release due to this mutation is not apparent (Schwer and Meszaros, 2000). The loop
213 containing S635A is in a similar conformation in this structure and in the structure of WT human

214 Prp22 (Felisberto-Rodrigues et al., 2019) (**Supplemental Fig. S6**). Part of the extensive N-
215 terminal domain of Prp22 is resolved and constitutes a long helix that bridges between the Prp22
216 RecA2 domain and the C-terminal domain of Cwc22; this helix was unassigned in previous P-
217 complex structures (**Fig. 4B**).

218 To improve the resolution of the peripheral, flexible regions, we used a new data-driven
219 regularization strategy (Kimanius et al., 2023) that allows focused refinements of much smaller
220 domains than previously possible (**Supplemental Fig. S4, S6**). Combined with AlphaFold2-
221 assisted modelling, we were able to obtain more accurate models for the U2 snRNP, NTC, U5
222 Sm ring, and Cwc22 N-terminal domains. Our model for the NTC within the P complex is similar
223 to our previous model for the NTC within C and C^i complexes (Wilkinson et al., 2021) (**Fig. 4C**).
224 Notably however, we observed a star-shaped density coordinated by several conserved lysines
225 from Clf1 and Ntc20, which we were able to model as inositol hexakisphosphate (IP_6) (**Fig. 4D**).
226 The same density, at lower resolution, is visible in the C complex (Wilkinson et al., 2021). A
227 distinct, separate IP_6 molecule had previously been observed within all catalytic spliceosomes
228 between the B^{act} and P-complex stages coordinated by Prp8 and (for C* and P-complexes) Slu7
229 (**Supplemental Fig. S6**). We do not believe that the NTC-bound IP_6 is essential for splicing since
230 deletion of the Clf1 tetratricopeptide repeat that coordinates IP_6 does not result in growth or
231 splicing phenotypes in yeast and Ntc20 is a non-essential splicing factor (Chen et al, 2001; Chung
232 et al., 1999). Nonetheless, it is possible that IP_6 may regulate splicing in some manner via
233 interactions with both Prp8 and the NTC.

234 We were able to unambiguously assign three, connected long α-helices to Fyv6 (**Fig. 4A**).
235 These helices were visible in previous cryo-EM reconstructions of yeast C* and P complexes but
236 were either unassigned or misassigned. In the cases of misassigned densities, Fyv6 was
237 previously attributed to the C-terminal domain of the 1st step factor Yju2 (Wilkinson et al., 2017).
238 Yju2 also has an elongated helical architecture and adopts a similar position on C complex
239 (Wilkinson et al., 2021) and the post-P complex Intron Lariat Spliceosome (ILS) (Wan et al., 2017).

240 We closely inspected the density from previously determined spliceosome structures and
241 concluded that the Yju2 C-terminus is still a better fit than Fyv6 for densities in B* and C
242 complexes, whereas Fyv6 is a better fit than Yju2 for densities in C* and P complexes
243 (**Supplemental Fig. S7**). Therefore, this position of Fyv6 seems to be characteristic of a 2nd step
244 conformation of the spliceosome and consistent with the position of its distant human homolog
245 FAM192A in the human pre-C* complex (Zhan et al., 2022).

246 Fyv6 makes a multitude of interactions with essential splicing factors (**Fig. 3B; 4E, F, G**).
247 One conserved region of Fyv6 is the N-terminus with a FVSE motif (**Supplemental Fig. S8**). This
248 motif forms a 'hook' that interacts with a hydrophobic patch on the surface of the Prp22 RecA2
249 domain, where it also forms hydrogen bonds by β-sheet augmentation (**Fig. 4E**). The hook is
250 followed by three α-helices. The start of helix 2 sits on top of the intron between the BP and the
251 active site docked 3' SS, where it may act as a steric block to prevent 3' SS undocking and
252 promote exon ligation (**Fig. 4F**) (Liu et al., 2017). Helix 2 also contains a patch of conserved
253 arginines that form salt bridges with Asp317 and Glu318 of Slu7 (**Fig. 4F**). The linker between
254 helices 2 and 3 interacts with the NTC component Cef1, and helix 3 interacts with NTC component
255 Syf1 (**Fig. 4G**). The binding interface with Syf1 overlaps with the Syf1/Yju2 interaction in the C
256 complex (Wilkinson et al., 2021), suggesting these interactions are mutually exclusive (**Fig. 4G**).
257 Fyv6 thus provides a direct link between the Prp22 ATPase, NTC components, and other essential
258 splicing factors over a distance of ~100 Å.

259 By 3D classification, we were able to resolve a total of three states of the P-complex
260 spliceosome (**Fig. 3C-E**). State I, represented by 51% of particles, is the most complete and has
261 all the above-described factors visible, including a stably-docked 3' SS. State II, represented by
262 20% of particles, is similar to State I but lacks density for the N-terminal half of the 2nd step factor
263 Slu7. The endonuclease-like domain of Prp8, to which this domain of Slu7 binds, is
264 correspondingly shifted. Interestingly, this state retains strong density for the 3' SS, suggesting

265 the N-terminal regions of Slu7 are not involved in maintaining 3' SS docking after exon ligation.
266 Finally, State III, containing 29% of particles, entirely lacks density for the 2nd step factors Slu7,
267 Prp18, and Fyv6. Prp17 and the RNase H domain of Prp8 are still present but are weaker than in
268 States I and II, suggesting they are more flexible in State III. Most of Prp22 can still be observed
269 with weaker density except for the C-terminal domain that interacts with Prp8, which lacks density
270 entirely. Importantly, State III also lacks density for the 3' SS but has density for the 3' exon,
271 suggesting it is indeed post-catalytic and represents a state after loss of 2nd step factors and
272 undocking of the 3' SS from the catalytic core. The coincidence of loss of Fyv6 with loss of Prp18
273 and Slu7 reinforces the notion that these three factors act together and are important for 3' SS
274 docking and stabilization of Prp17, Prp22, and the RNase H domain of Prp8.

275 **The Fyv6/Syf1 Interaction is Critical for Suppressing *fyv6Δ* Phenotypes**

276 To determine the functionally critical regions and interactions of Fyv6, we used the cryo-
277 EM structure to design five truncation mutants (**Fig. 5A**). The first three truncations remove amino
278 acids from the N-terminus of Fyv6: deletion of the first 16 amino acids, which are not resolved in
279 the cryo-EM structure (Δ1-16); deletion of the first 23 amino acids, which removes the conserved
280 hook region of Fyv6 that interacts with the Prp22 RecA2 domain (Δ1-23); and deletion of amino
281 acids 1 to 51, which additionally removes the first α-helix and interactions with Prp22, Prp8, and
282 Slu7 (Δ1-51). The remaining two mutants are C-terminal truncations. In the first, amino acids 134
283 to 173, which do not have clear density in the cryo-EM structure and are not modeled but which
284 do contain a predicted nuclear localization signal (NLS), are deleted (Δ134-173) (Nguyen Ba et
285 al., 2009). In the second, amino acids 103 to 173 are deleted (Δ103-173), which additionally
286 removes the region of the protein that interacts with Syf1.

287 We tested each truncation mutant for its ability to suppress the *cs* and *ts* phenotypes of
288 the *fyv6Δ* strain when expressed from a plasmid under the native promoter (**Fig. 5B**). All of the N-
289 terminal truncation mutations could suppress the *cs* or *ts* phenotypes to some degree.

290 Surprisingly, a strain with the complete deletion of the conserved hook domain that interacts with
291 Prp22 (Δ1-23) grew similarly to the strain expressing WT Fyv6. We wondered if splicing changes
292 could still be present even if the growth phenotype was suppressed; so, we assayed *SUS1*
293 isoforms by RT-PCR. We previously showed that loss of Fyv6 causes use of an alternative 3' SS
294 in the first intron of this pre-mRNA (Lipinski et al., 2023). In addition to suppression of the *fyv6Δ*
295 growth phenotype, the N-terminal truncation mutants also showed no evidence for changes in
296 *SUS1* splicing (**Fig. 5C**). The N-terminal region of Fyv6 composed of the hook domain and the
297 first α-helix is not required for suppression of either the temperature sensitivity or splicing
298 phenotypes observed when Fyv6 is lost despite its conservation and interactions with critical
299 splicing factors (Prp8, Prp22, and Slu7).

300 For the C-terminal truncations, the Δ134-173 truncation was also able to suppress the *cs*
301 and *ts* phenotypes, indicating that the predicted NLS is also not essential (**Fig. 5B**). However, this
302 mutant grew more poorly at 16°C than did the Δ1-16 and Δ1-23 truncations and showed some
303 evidence of alternative 3' SS usage in *SUS1* (**Fig. 5C**). The largest effects were seen when the
304 C-terminus was truncated further. The Δ103-173 truncation strain phenocopied the *fyv6Δ* strain
305 and grew poorly at 37°C and was dead at 23° or 16°C (**Fig. 5B**). Additionally, RT-PCR showed
306 increased use of the alternative 3' SS in *SUS1* with this truncation (**Fig. 5C**). To determine if this
307 phenotype could be due to loss of protein expression, we assayed expression of the epitope-
308 tagged proteins by western blot (**Supplemental Fig. S9A**). In all cases, we could detect protein;
309 however, the abundance of the N-terminally epitope-tagged Δ103-173 variant was much lower
310 than the others. Therefore, we also constructed a C-terminally epitope-tagged version of Δ103-
311 173 (**Supplemental Fig. S9B**). The C-terminally-tagged protein expressed at much higher levels
312 but also failed to suppress the *cs* and *ts* phenotypes. These data suggest that the C-terminal
313 region of Fyv6 that includes a portion of α-helix 3 and the Syf1 interaction domain is critical for
314 function.

315 To obtain additional evidence for the importance of the Fyv6/Syf1 interaction, we created
316 a *syf1Δ* shuffle strain containing WT Fyv6 and expressed C-terminal Syf1 truncations (**Fig. 5D**).
317 We hypothesized that loss of the Fyv6-interacting domain on Syf1 would phenocopy *fyv6Δ*. We
318 observed just this effect. Loss of the Fyv6-interacting region in Syf1 Δ778-859 and Δ634-859
319 mutants resulted in either modest (Δ778-859) or severe (Δ634-859) *cs* and *ts* phenotypes. In
320 addition, these Syf1 truncation mutants also triggered use of the alternative 3' SS in *SUS1* (**Fig.**
321 **5F**). Interestingly, if the Δ778-859 and Δ817-859 Syf1 mutants are expressed in a *fyv6Δ*
322 background, it results in suppression of the *fyv6Δ ts* phenotype (**Fig. 5G; *c.f.* Fig. 5B**). However,
323 the *SUS1* alternative 3' SS is still used (**Fig. 5H**). This indicates that *ts* phenotype suppression
324 and triggering usage of the alternative 3' SS in *SUS1* are separable processes.

325 As mentioned above, the Syf1/Fyv6 interaction is mutually exclusive with the Syf1/Yju2
326 interaction that occurs during 5' SS cleavage and is reformed in the ILS spliceosome. One
327 possible explanation for suppression of the *ts* phenotype in *fyv6Δ*/*syf1*(Δ778-859 or Δ817-859)
328 strains is that Fyv6 and Yju2 are competing with one another and binding of either protein to the
329 wrong spliceosome complex results in growth and splicing defects. When the Yju2/Fyv6 binding
330 site on Syf1 is removed, the observed phenotypes could be due to failure of Yju2 to be properly
331 recruited to the P complex spliceosome for displacement of Fyv6. However, recruitment occurs
332 correctly when Fyv6 is deleted since it no longer needs to be displaced. Similarly, phenotypes
333 due to loss of Fyv6 could arise from retention of Yju2 during exon ligation. A prediction of this
334 model is that failure to properly remove or recruit Yju2 and Fyv6 can result in similar phenotypes.
335 Further work will be needed to understand the binding dynamics of these factors.

336 **Mutations in Many Different Splicing Factors Can Suppress *fyv6Δ* Phenotypes**

337 To gain additional insights into Fyv6 function, we carried out a genetic screen to detect
338 spontaneously arising suppressors that can correct temperature-dependent growth defects (**Fig.**
339 **6A**). This method has previously been used to illuminate many aspects of spliceosome

340 biochemistry and non-silent mutations within splicing factors are likely causative for suppression
341 (Montemayor et al. 2014; Kuhn and Brow, 2000; Brow, 2019).

342 We plated saturated *fyv6Δ* yeast cultures onto 20 different YPD plates and incubated them
343 at 37°C until colonies arose. Within several days, colonies of various sizes appeared and were
344 isolated. A subset of picked colonies were then tested for suppression of the *ts* phenotype. All of
345 these colonies were able to suppress growth defects at 37°C, and many also suppressed the *cs*
346 phenotype at 23°C (**Supplemental Fig. S10**). We then performed whole genome sequencing on
347 the largest of the picked colonies as these were expected to be the strongest suppressors. In 19
348 of 20 sequenced strains, we were able to identify at least one non-silent mutation in a splicing
349 factor (**Fig. 6B**, **Supplemental Table S5**). When we carried out a similar experiment aimed at
350 identifying *cs* suppressors, we were unable to identify any likely causative mutations in splicing
351 factors. Therefore, we focused our analysis on the *ts* suppressor mutations.

352 Collectively, the identified mutations tended to fall into two categories: gain of positive
353 charge or substitution with a bulkier side chain. Gain of positive charge mutations were found in
354 Prp8 (G1868R) as well as the second step factors Slu7 (A24R, and N28K), and Prp22 (I1133R).
355 Structurally, amino acids within Prp8 and Prp22 are proximal to RNA within the spliceosome and
356 addition of charged amino acid side chains may stabilize interactions with the phosphodiester
357 RNA backbone. The N-terminus of Slu7 containing A24 and N28 is not resolved in any
358 spliceosome structure to our knowledge and normally contains many negatively charged
359 residues. The majority of identified suppressors involve a mutation to a bulkier side chain including
360 several in Prp8 (S1594F/Y, V1862L), Prp17 (A251V, G386W), Cef1 (A37V), and Clf1 (T33I). The
361 increase in hydrophobic surface area provided by these mutations may help to stabilize
362 interactions with nearby proteins, compensating for structural destabilization due to the absence
363 of Fyv6.

364 We isolated one suppressor mutation within the U2 snRNA (A25G) near where the C-
365 terminal domain of Prp22 inserts towards the active site and located beneath the Fyv6 binding

366 site. It has previously been observed that mutation of this specific U2 snRNA nucleotide is not
367 deleterious to growth (McPheeters and Abelson, 1992), and is therefore well-tolerated by yeast.
368 The mechanism of suppression by this mutation is not clear; however, it is interesting to note that
369 we also observed suppressor mutations in the U2 snRNP component Rse1 (**Supplemental Table**
370 **S5**) which is released from the spliceosome prior to catalysis. The Rse1 mutations always
371 occurred coincident with mutations in other splicing factors. It is possible that suppressors in
372 factors present prior to or after exon ligation are able to suppress (or enhance suppression of)
373 *fyv6Δ* by changing how pre-mRNAs compete for a limited set of splicing factors or by reducing
374 blocks to pre-spliceosome assembly caused by accumulation of stalled complexes (Mendoza-
375 Ochoa et al., 2019; Munding et al., 2013). Together these data indicate that mutations in many
376 different splicing factors including second-step factors and the U2 snRNA can be isolated from
377 *fyv6Δ* suppressor strains.

378 **Multiple Second-step Splicing Defects can be Rescued by the Same Suppressor**

379 We decided to study several of these mutations in greater detail and to confirm that they
380 were sufficient for *fyv6Δ ts* phenotype suppression. In the case of Cef1, we obtained several
381 mutants located near the interface between Cef1 and the 2nd step factor Prp17: A37V, M175I, and
382 Q193P (**Fig. 6C**). This interface has only been observed in structures of C* and P-complex
383 spliceosomes, suggesting its importance for exon ligation. In addition, it has previously been
384 reported that another mutant of Cef1 A37, A37P, is able to suppress splicing defects due to a BS
385 adenine to guanosine substitution (BS-G) which causes stalling after 5' SS cleavage (Query and
386 Konarska, 2012). Therefore, we wondered if other Cef1 mutants capable of suppressing defects
387 due to BS-G could also suppress *fyv6Δ* (Cef1 A37P, V36R, and S48R). We created *fyv6Δ* shuffle
388 strains for Cef1 and tested each mutant's ability to suppress *cs* and *ts* phenotypes (**Fig. 6D**). All
389 of these Cef1 mutants, both those isolated from our suppressor screen and those identified as
390 BS-G suppressors, could at least weakly suppress the *cs* phenotype at 23°C with our isolated
391 M175I mutant being a particularly strong suppressor. In addition, all of the mutants except Cef1

392 A37V could suppress the *ts* phenotype at 37°C to varying degrees. These results confirm that
393 single point mutants in Cef1 can suppress *fyv6Δ* growth phenotypes and that at least some BS-
394 G suppressors in Cef1 also suppress *fyv6Δ*. A common mechanism could be that these mutations
395 stabilize the exon ligation conformation of the spliceosome to favor the 2nd step either when a
396 BS-G is present or Fyv6 is absent.

397 In the case of Prp8, we tested five different suppressor mutations in *prp8* shuffle strains
398 (**Fig 6E,F**). Identification of mutants in Prp8 that suppress *fyv6Δ* is not surprising since many
399 different alleles of Prp8 are known to modulate the conformational equilibrium between the 1st
400 and 2nd steps (Fica and Nagai, 2017; Liu et al., 2007; Query and Konarska, 2004). We previously
401 discovered that one Prp8 2nd step allele, P986T, could suppress a *fyv6Δ* growth defect (Lipinski
402 et al., 2023).

403 We identified two suppressors within the Prp8 α-finger domain at position S1584 and
404 another three within the Rnase H-like domain (**Fig. 6E, Supplemental Table S5**) (Galej et al.
405 2013). S1584 is located adjacent to a residue that crosslinks with the BP (aa 1585) (Galej et al.,
406 2013). Proximity to the BP suggests that mutations at S1584 might destabilize RNA bound within
407 the active site after branching, alleviating the stall caused by *fyv6Δ* after the 1st step or facilitating
408 formation of the 2nd step conformation.

409 Suppressors of other splicing defects have been previously identified within the Prp8
410 RNase H-like domain, two of which are located at the same position as *fyv6Δ* suppressors.
411 V1862A/Y/D and T1982A were identified as suppressors of, respectively, the *U4-cs*1 allele (Kuhn
412 and Brow, 2000; Kuhn et al., 1999) or the 5' SS U2A mutant (Siatecka et al., 1999). V1862 is
413 located within the RNase H-like domain β-finger (**Fig. 6E**), while T1982 is located at the base of
414 the β-finger (**Fig. 6C**). We identified *fyv6Δ* suppressors at both V1862 (V1862L) and T1982
415 (T1982S) as well as a third suppressor (G1868R), also located in the β-finger. Several 2nd step
416 Prp8 alleles are also located proximal to G1868 (N1869D and V1870N) (Query and Konarska,
417 2004).

418 Four of the identified Prp8 suppressor mutations could partially suppress either or both of
419 the *cs* and *ts fyv6Δ* phenotypes (**Fig. 6F**). Prp8 S1574Y, V1862L, G1868R, and T1982S
420 suppressors were able to support growth at 37°C. Prp8 V1862L and T1982S also partially
421 suppressed the growth defects at 16 and 23°C. Even though we isolated the Prp8 S1584F mutant
422 in our screen and this substitution is very similar to S1584Y, we were not able observe
423 suppression due to this mutant in these strains. Mutations within the Prp8 β-finger are able to
424 compensate for loss of Fyv6 and these mutations are located near known Prp8 2nd step alleles.
425 As with Cef1 mutants, it is possible that *fyv6Δ* suppression is originating from stabilization of the
426 2nd step conformation.

427 Finally, given our observations with the Cef1 and Prp8 mutants, we wondered about the
428 generality of 2nd step splicing factor suppression. Several dominant mutants in the 2nd step factor
429 Prp18 were previously shown to suppress *ts* phenotypes due to various mutations in Slu7
430 (Aronova et al., 2007). We wondered if these Prp18 mutants would also suppress the *ts* (or *cs*)
431 phenotype due to Fyv6 loss. Indeed, the Prp18 V191A suppressor of *slu7* alleles was able to
432 improve growth at 37°C of *fyv6Δ* yeast (**Supplemental Fig. S11**). Together our results from the
433 suppressor analysis support a model in which a given 2nd step suppressor mutation may be able
434 to restore splicing activity lost by a variety of mechanisms.

435 **A Prp22-Dependent Splicing Stall is Relieved by Fyv6 Deletion**

436 The final *fyv6Δ* suppressor mutation that we studied was the Prp22 I1133R mutant. This
437 mutation is located within the C-terminal domain of Prp22 that enters the spliceosome active site
438 and is located proximal to U2 snRNA nucleotide A31 (**Fig. 7A**). Fyv6 bridges over this Prp22-U2
439 snRNA interaction. The I1133R mutation might stabilize Prp22/U2 snRNA contacts that can
440 compensate for Fyv6 loss and promote exon ligation. The Prp22 I1133R mutant is able to weakly
441 suppress both the *cs* and *ts* phenotypes in *fyv6Δ* yeast (**Fig. 7B, C**). Given its location in the C-
442 terminal domain, we wondered if it or *fyv6Δ* would show synthetic genetic interactions or epistasis

443 with mutations in the helicase domain. We tested two helicase domain mutations, R805A and
444 G810A, both of which are known to impact Prp22-dependent proofreading (Mayas et al., 2006).
445 The Prp22 R805A mutant is by itself *cs* (Schwer and Meszaros, 2000) and showed a synthetic
446 lethal interaction with *fyv6Δ* (**Fig. 7B, 7C**). This was only slightly rescued by simultaneously
447 introducing I1133R into Prp22. In contrast, Prp22 G810A mutant is viable in the presence and
448 absence of Fyv6 as well as in combination with the I1133R suppressor mutation (**Fig. 7B, 7C**).
449 Prp22 G810A by itself does not suppress the *ts fyv6Δ* phenotype; however, the Prp22
450 G810A/I1133R double mutant is a stronger suppressor of the *ts* phenotype than either mutant
451 alone. These additive genetic interactions suggest that the Prp22 *fyv6Δ* suppressor mutation
452 (I1133R) and the helicase domain mutations (R805A and G810A) impact distinct Prp22 functions.
453 These functions could correspond to Prp22's role in promoting exon ligation during the 2nd step
454 (the C-terminal domain mutation) and its role in promoting ATP-dependent mRNA release and
455 proofreading (the helicase domain mutations).

456 Recently, it was reported that the Prp22 G810A mutant could activate usage of some
457 alternative 3' SS that are also activated by *PRP18* deletion (Roy et al., 2023). We therefore
458 wondered if any of the Prp22 mutants could activate alternative 3' SS also activated by *FYV6*
459 deletion. We isolated RNA from these strains and analyzed *SUS1* splicing by RT-PCR (**Fig. 7D,**
460 **E**). None of the Prp22 mutants activated usage of the *SUS1* alternative 3' SS or enhanced usage
461 of this site beyond what is observed upon Fyv6 deletion. However, we noticed that the Prp22
462 helicase mutants, R805A and G810A, both caused an accumulation of unspliced pre-mRNA. This
463 is consistent with these mutations causing a block during pre-mRNA splicing and having a
464 different effect on splicing than Prp22 I1133R. Surprisingly, the block due to the G810A mutation
465 was relieved in the *fyv6Δ* strains and little pre-mRNA accumulation was observed in the absence
466 of Fyv6. This result suggests that Fyv6 could act as a negative regulator of splicing of the *SUS1*

467 transcript when a Prp22 helicase domain mutant is present. Removing Fyv6 restores splicing by
468 activation of the *SUS1* BP proximal 3' SS.

469 To further explore the connections between Fyv6 and Prp22 fidelity, we used the ACT1-
470 CUP1 assay in which yeast growth in the presence of increasing concentrations of Cu^{2+} is
471 proportional to the extent of splicing of a reporter RNA (**Fig. 7F, G**; **Supplemental Fig. S12, S13**).
472 Since the Prp22 R805A mutant grew poorly, we only assayed the Prp22 G810A, I1133R, and
473 G810A/I1133R (double) mutants in the presence and absence of Fyv6. Consistent with previous
474 results, we found that *fyv6Δ* is deleterious for splicing of the WT ACT1-CUP1 reporter containing
475 consensus splice sites. Copper tolerance was improved when *fyv6Δ* was combined with Prp22
476 I1133R. Unexpectedly, Prp22 I1133R was actually deleterious when Fyv6 was present for this
477 reporter. If this Prp22 mutant and Fyv6 both promote the 2nd step, then their combination may
478 have an additive, negative effect on splicing due to over-stabilization of this spliceosome
479 conformation.

480 Finally, we assayed strains containing a 3' SS UAG to gAG reporter since it was previously
481 shown that Prp22 helicase domain mutants could increase usage of nonconsensus 3' SS due to
482 faulty proofreading activity (**Fig. 7F, G**). In agreement with this, we observed a dramatic increase
483 in copper tolerance when Prp22 contained both the C-terminal domain and helicase mutants
484 (double). This suggests that splicing of nonconsensus 3' SS splice sites is enhanced both by
485 stabilization of the 2nd step conformation (I1133R) and perturbing mRNA release (G810A). This
486 effect on Prp22 is Fyv6-dependent since loss of Fyv6 results in very poor copper tolerance of
487 strains containing the gAG reporter, likely since this 3' SS is located far from the BP (38 nt). These
488 results show that *fyv6Δ* can be suppressed with a Prp22 C-terminal domain mutant and that
489 mutations in the Prp22 C-terminal domain can have distinct functional consequences from those
490 located in the helicase domain. In the case of *SUS1*, stalling of splicing due to the Prp22 G810A
491 mutant can be relieved by removing Fyv6 and activation of a BP proximal 3' SS.

492 **DISCUSSION**

493 Here, we establish Fyv6 as a 2nd step splicing factor in yeast that promotes usage of BP-
494 distal 3' SS. Structural, genetic, and biochemical studies reveal critical contacts and interactions
495 between Fyv6 and the splicing machinery. From these data, we propose that Yju2/Syf1
496 interactions need to be disrupted for proper Fyv6 recruitment and that Fyv6 can enforce the
497 Prp22-dependence of at least some splicing events. Combined, our data allow us to propose a
498 model for Fyv6's role during the 2nd step (**Fig. 7H**). In this model, Fyv6 is recruited to the C*
499 complex after Prp16-dependent release of Yju2, which exposes the binding site for Fyv6 on Syf1.
500 Once bound, Fyv6 (possibly in concert with Slu7 and Prp18) facilitates docking of BP distal 3' SS
501 into the active site. In the absence of Fyv6, the use of BP distal 3' SS becomes more difficult and
502 BP proximal 3' SS are favored. Under these conditions, the requirement for Prp22 during exon
503 ligation is reduced and Yju2 may also potentially rebind Syf1. One or both of these factors could
504 contribute to formation of a lower fidelity spliceosome with relaxed sequence constraints for exon
505 ligation.

506 **Structural Insights into the Recruitment and Release of 2nd step Factors**

507 A key principle of spliceosome structural biochemistry is the presence of mutually
508 exclusive interactions that coordinate the stepwise and directional progression of splicing
509 (Townsend et al., 2020). Our cryo-EM structure of the P complex spliceosome suggests another
510 such interaction is involved in the 1st to 2nd-step transition during which Fyv6 displaces Yju2. Yju2
511 and Fyv6 occupy overlapping binding sites on the splicing factor Syf1 and, in fact, unassigned
512 density in spliceosome P complexes due to Fyv6 was previously mis-interpreted as Yju2 due to
513 their structural similarity (Wilkinson et al., 2017; Wilkinson et al., 2021). We propose that Prp16-
514 promoted spliceosome remodeling results in release of Yju2 from the spliceosome C complex and
515 permits mutually exclusive binding of Fyv6. Fyv6 remains bound in the P complex but then
516 dissociates to permit re-binding of Yju2 in the ILS complex.

517 Previously, Chiang and Cheng noted that while the N-terminal half of Yju2 was able to
518 restore 1st step activity to Yju2-depleted extracts, it is much more stably associated if a second
519 polypeptide containing the C-terminal, Syf1-interacting half was included (Chiang and Cheng,
520 2013). It is possible that competition between Yju2 and Fyv6 for Syf1 binding can explain these
521 results. If only the N-terminal half of Yju2 is present, Fyv6 could associate prematurely with Syf1
522 and result in destabilization of the 1st step conformation in favor of 2nd step interactions. This may
523 then result in weaker binding for the N-terminal half of Yju2. Failure to properly recruit and
524 exchange the Yju2/Fyv6 interaction on Syf1 may also be the origin of some of the yeast growth
525 and splicing phenotypes we observe (**Fig. 5**).

526 The need for Yju2/Fyv6 exchange hints at two distinct functions for Fyv6: a role in Yju2
527 displacement to prevent its re-binding during exon ligation and a role in stabilization of the 2nd
528 step spliceosome conformation. These two functions can potentially result in the distinct *cs* and
529 *ts* phenotypes in yeast. While more work is needed to dissect these phenotypes, it is possible that
530 the *cs* phenotype results from increased stability of the Yju2/Syf1 interaction at lower
531 temperatures and the need for Fyv6 to act as a competitor of this interaction. The *ts* phenotype
532 on the other hand may result from destabilization of the 2nd step conformation of the spliceosome
533 active site due to loss of Fyv6. It is possible that loss of Fyv6 results in destabilization due to
534 removal of a buttress that holds the RNase H-like domain of Prp8 in place (along with Prp18),
535 changes in how the C-terminal domain of Prp22 interacts with the spliceosome active site,
536 removal of an impediment to reversal of the U2 snRNA/BS duplex conformational change that
537 occurs during the C to C* complex transition, or a combination of these factors.

538 The high quality of our cryo-EM data combined with 3D classification also provide new
539 insights into the requirements for 3' SS docking into the active site and potentially for how the P
540 complex spliceosome is disassembled into the ILS complex. It was previously speculated that the
541 N-terminal domain of Slu7 may be critical for 3' SS docking by reducing the entropic cost of this
542 process when the BP to 3' SS distance is long (Wilkinson et al., 2017). In our state II P complex

543 structure, the 3' SS remains docked but this domain of Slu7 is not observed. This suggests that
544 either Slu7 N-terminal domain interactions with Cwc22 and Prp8 are not essential for 3' SS
545 docking into the active site for exon ligation and/or that these interactions are not essential for
546 maintaining 3' SS docking within P complex once they form in C*.

547 In the state III P complex structure, densities for the 2nd step factors Fyv6, Prp18, and Slu7
548 are entirely missing and the 3' SS is no longer docked into the active site. This result suggests
549 that 3' SS undocking is coupled to 2nd step factor release. Prp22 is still present in this structure,
550 and it is possible that state III represents a conformation occurring after exon ligation but prior to
551 Prp22-dependent mRNA release. In this case, the state III structure implies that Prp22 ATPase
552 activity is not needed for dissociation of Fyv6, Prp18, and Slu7. It is also interesting to note that
553 the C-terminal domain of Prp22 can no longer be resolved in the state III structure. What exactly
554 activates the Prp22 ATPase to promote proofreading or mRNA release is not known. It is
555 conceivable that undocking of the 3' SS from the active site can be sensed by the Prp22 C-
556 terminal domain and this contributes to ATPase activation. This model differs from that previously
557 proposed for Prp22-enabled 3' SS sampling in which that ATPase activity of Prp22 is needed to
558 undock the 3' SS (Semlow et al., 2016). However, sampling could involve multiple steps: ATP-
559 independent 3' SS undocking and ATP-dependent entry into the sampling state. Whether or not
560 the 2nd step factors must release or alter conformation to enable sampling is unknown. Regardless
561 of the exact mechanism, it is important to recognize that the P complex structures determined
562 here were all obtained using a Prp22 mutant defective in mRNA release. The chemical and kinetic
563 competencies of these states will require future investigations.

564 **Multiple, Non-Redundant 2nd Step Factors Promote Use of BP Distal 3' SS**

565 The challenge of 3' SS selection involves not just selection of the correct nucleotide
566 sequence (YAG) but also identifying which YAG sequence to use. Here, we define a function for
567 Fyv6 in facilitating use of BP distal 3' SS, especially those located $\geq$ 21 nt away from the branch.
568 This function is similar to those of other 2nd step factors important for efficient splicing when the

569 BP-3' SS distance is ≥12 nt (Slu7, Prp18) or ≥21 nt (Prp22) (Brys and Schwer, 1996; Schwer and
570 Gross, 1998; Zhang and Schwer, 1997). Human Slu7 has additionally been reported to be
571 important for preventing suppression of the correct 3' SS in favor of up- or downstream alternative
572 3' SS (Chua and Reed, 1999). Our previous study using competing 3' SS in the ACT1-CUP1
573 intron did not provide evidence for suppression of the correct 3' SS in the absence of Fyv6,
574 suggesting that this function is not shared between human Slu7 and yeast Fyv6. Nonetheless, it
575 is important to recognize that the splicing machinery employs multiple factors that enforce usage
576 of BP distal 3' SS. These functions are not redundant as changes in 3' SS are still observed in the
577 absence of Fyv6 but presence of Prp18 and vice versa (Roy et al., 2023).

578 Intron architecture can also contribute to 3' SS selection since canonical "AG" 3' SS are
579 depleted in humans in the region between the BP and annotated 3' SS (the AG exclusion zone,
580 or AGEZ) (Corvelo et al., 2010; Gooding et al., 2006). AG sites are also typically depleted in the
581 corresponding region in yeast introns (data not shown). This would suggest that annotated 3' SS
582 are also the most optimal sites located downstream of the BP. However, an important assumption
583 of this model is that non-AG 3' SS can also be effectively proofread and not used. Deletion of
584 either Prp18 or Fyv6 leads to activation of not just BP proximal 3' SS but also those with highly
585 divergent sequences from the YAG consensus (Roy et al., 2023). This suggests that an AGEZ
586 alone is insufficient for correct 3' SS usage and that mechanisms to ensure preferential use of
587 YAG sites are critical.

588 It is likely that Fyv6 and Prp18 enforce usage of YAG sites by common as well as factor-
589 specific mechanisms. Both proteins stabilize the conformation of the Prp8 RNase H-like domain
590 in P complex. Numerous splice site suppressor mutations map to this domain including those that
591 enhance splicing of non-YAG 3' SS (Galej et al., 2013). Fyv6 and Prp18 may be essential for
592 establishing a "high fidelity" conformation of the RNase H-like domain that enforces use of
593 canonical YAG 3' SS and preventing activation of cryptic sites within the AGEZ. In support of this,

594 we note that in our state III P complex structure that lacks both Fyv6 and Prp18 and a stably
595 docked 3' SS, the RNase H-like domain is also more flexible.

596 In addition to this possibility, Fyv6 and Prp18 may also contribute uniquely to 3' SS fidelity
597 and selection. The conserved loop region of Prp18 inserts into the spliceosome active site and
598 contacts the 3' SS. Partial deletion of this region of Prp18 phenocopies at least some of the
599 changes in 3' SS selection when Prp18 is deleted entirely (Crotti et al., 2007; Roy et al., 2023).
600 This indicates that even when the Prp8 RNaseH-like domain is still stabilized by Prp18 (and Fyv6)
601 disruptions to 3' SS selection can still occur. Unlike Prp18, Fyv6 does not contact the spliceosome
602 active site. However, it is the only 2nd step factor that contacts exon ligation fidelity factor Prp22.
603 While these contacts are not essential for suppressing use of an alternative 3' in *SUS1*, a mutation
604 in Prp22 can nonetheless suppress a *fyv6Δ* phenotype and loss of Fyv6 relieves a Prp22 helicase
605 mutant-dependent stall in *SUS1* splicing. These observations suggest that Fyv6 and Prp22 are
606 functionally connected to one another.

607 **Some 2nd Step Factors May Enforce Usage of Prp22 during Exon Ligation**

608 We were particularly struck by the similarities in the BP-3' SS distances for the requirement
609 of Prp22 during exon ligation and for promotion of BP distal 3' SS usage by Fyv6, both $\geq$21 nt
610 (Schwer and Gross, 1998). In addition, the alternative, BP proximal 3' SS that are activated when
611 Fyv6 is deleted show much less sequence conservation relative to the annotated 3' SS and
612 include sequences (GAG, BG) known to be proofread and rejected by Prp22. Together, this
613 suggests that one function of Fyv6 is to enforce Prp22-dependence of exon ligation by stabilizing
614 a spliceosome conformation that more easily enables usage of BP distal 3' SS (**Fig. 7H**). As these
615 sites require Prp22 for exon ligation, it is also likely that they are subject to Prp22-dependent
616 proofreading, and this may enforce accurate exon ligation at the YAG 3' SS consensus. When
617 Fyv6 is absent, many alternative, BP proximal 3' SS are activated. These sites could have a
618 relaxed requirement for Prp22 and proofreading. While the Fyv6-dependence of Prp22 occupancy
619 is beyond the scope of the current manuscript, loss of Prp18 (which also activates usage of non-

620 canonical, BP-proximal 3' SS) does result in lower occupancy of Prp22 on the *ACT1* intron
621 (Strittmatter et al., 2021). This suggests that Prp22 occupancy, and possible involvement in the
622 exon ligation step, can be influenced by 2nd step factors.

623 There is precedent for nonessential splicing factors enforcing use of a proofreading
624 ATPase. Cus2 is not essential for pre-spliceosome formation (Yan et al., 1998). However, when
625 Cus2 is present then ATPase activity of Prp5 is essential for disruption of the Hsh155/Cus2
626 interaction (Perriman et al., 2003; Talkish et al., 2019). In this case, Cus2 is not essential for Prp5
627 proofreading of BP selection, and the connection between the ATP hydrolysis activity of Prp5,
628 removal of Cus2, and proofreading is unclear (Liang and Cheng, 2015; Talkish et al., 2019; Xu
629 and Query, 2007). It is possible that enforcement of Prp5 ATPase activity by Cus2 is important for
630 other aspects of pre-spliceosome formation *in vivo* and the impact of Prp5 and Cus2 on BP
631 selection has not yet been studied transcriptome-wide using high-resolution, sequencing-based
632 approaches. The C-terminal domain of the 1st step splicing factor Yju2 (the same domain that
633 competes with Fyv6 for Syf1 binding) is also not essential for 5' SS cleavage. In the absence of
634 this domain, the N-terminal domain of Yju2 is sufficient for promoting the 1st step reaction, and
635 the spliceosome can transition to the 2nd step and carry out exon ligation without Prp16, albeit
636 inefficiently (Chiang and Cheng, 2013). Importantly, addition of the C-terminal domain on a
637 separate polypeptide reduces Prp16-independent activity. This suggests that the Yju2 C-terminal
638 domain enforces the use of the Prp16 ATPase. As we propose with Fyv6 and Prp22, the C-
639 terminal domain of Yju2 may not just help to promote the 1st to 2nd step transition by enforcing
640 Prp16-dependence but could also facilitate Prp16-dependent proofreading during 5' SS cleavage
641 (Koodathingal et al., 2010; Semlow et al., 2016). General operating principles of the yeast splicing
642 machinery may not just include proofreading but also use of splicing factors that enforce usage
643 of the proofreading ATPases.

644

645 **MATERIALS AND METHODS**

646 The yeast strains and plasmids used in this study are described in **Supplemental Tables**
647 **S6 and S7**. Yeast transformation, plasmid shuffling/5-FOA selection, and growth were carried out
648 using standard techniques and media (Treco and Lundblad 1993; Sikorski and Boeke 1991).

649 **Cryo-electron microscopy**

650 Purification of dominant-negative Prp22

651 Yeast Prp22 with a dominant-negative S635A mutation was cloned into pRS424 and
652 pRS426 vectors after an N-terminal CBP-His-TEV tag (Galej et al., 2013). The protein was
653 expressed in 24 L of BCY123 yeast cells essentially as described (Galej et al., 2013).
654 Recombinant Prp22 was then purified first by Calmodulin-Sepharose in a buffer containing 50
655 mM Tris-HCl pH 8.5, 350 mM NaCl, 2 mM $CaCl_2$, 1 mM Mg acetate, 1 mM imidazole, 0.1% NP-
656 40 substitute, 5 mM β-mercaptoethanol and eluted with 3 mM EGTA. The protein was dialyzed
657 into 20 mM Tris-HCl pH 7.4, 350 mM NaCl, 10 mM imidazole, 0.1% NP-40 substitute and further
658 purified over Ni-NTA resin at 500 mM NaCl and eluted with 200 mM imidazole. The eluted protein
659 was treated with His-tagged TEV protease during dialysis against 20 mM HEPES-KOH pH 7.9,
660 300 mM KCl, 0.2 mM EDTA, 20% glycerol, 0.5 mM DTT, before removal of the protease with Ni-
661 NTA resin. The final protein was frozen in liquid nitrogen and stored at -80 °C.

662 Preparation and purification of P complex for cryo-EM

663 P complex was purified as described in (Wilkinson et al., 2017). Brr2-TAPS yeast were
664 grown in a 120 L fermenter and splicing extract was prepared by the liquid nitrogen method
665 essentially as previously described (Lin et al., 1985). A pre-mRNA substrate consisting of 20 nt
666 5'-exon, 95 nt intron, and 32 nt 3'-exon from the UBC4 pre-mRNA followed by 3xMS2 stem loops
667 was generated by run-off in vitro transcription from an EcoRI-linearized plasmid template. The
668 RNA product was labelled at the 3' end with fluorescein-5-thiosemicarbazide (Wu et al., 1996). A
669 180 mL in vitro splicing reaction was performed containing 60 mM potassium phosphate pH 7, 2
670 mM ATP, 2.5 mM $MgCl_2$, 3% w/v PEG8000, 3 nM pre-mRNA, 37.5 nM MS2-MBP protein, and

671 40% (v/v) splicing extract treated with dominant negative Prp22 S635A. Reactions were incubated
672 for 30 min at 23°C, then incubated for 20 min with 5 mM of a DNA oligonucleotide complementary
673 to the 3'-exon (oligo sequence 5'-ATGAAGTAGGTGGAT-3') to induce cleavage of the 3'-MS2 tag
674 by the endogenous RNase H activity of the splicing extract. The reaction mixture was centrifuged
675 through a 40% glycerol cushion in buffer A (20 mM HEPES, pH 7.9, 75 mM KCl, 0.25 mM EDTA).
676 The cushion was collected and applied to amylose resin in the presence of 0.025% NP-40
677 substitute. After overnight incubation at 4ºC the resin was washed and eluted with buffer A
678 containing 5% glycerol, 0.01% NP-40 substitute and 12 mM maltose. Fractions containing
679 spliceosomes were concentrated to 0.1 mg/mL then dialyzed against buffer A for 3 h.

680 For cryo-EM grid preparation, a freshly glow-discharged Cu300 R2/2 holey carbon grid
681 with a 2-nm layer of amorphous carbon (Quantifoil) was mounted in the chamber of a Vitrobot
682 Mark IV (Thermo Fisher Scientific) maintained at 4°C and 100% humidity. Spliceosomes (3 µL)
683 were applied and after 60 s was manually blotted using Ø55 grade 595 filter paper (Ted Pella),
684 followed by application of another 3 µL of spliceosomes, waiting 60 s, before blotting again and
685 plunging into liquid ethane.

686 Cryo-EM data collection

687 Cryo-EM data were collected as two datasets from two grids made from the same sample.
688 Dataset 1 was acquired using a Thermo Scientific Titan Krios cryo-TEM (LMB Krios 1) and dataset
689 2 was acquired using a Thermo Scientific Titan Krios G3i cryo-TEM (LMB Krios 3). Both used a
690 K3 direct detector (Gatan) operated in super-resolution mode with 2-fold binning, and an energy
691 filter with slit width of 20 eV. Micrographs were collected automatically using EPU in AFIS mode,
692 yielding a total of 51,113 movies at 81,000x or 130,000x magnification with a real nominal pixel
693 size of 0.93 Å or 0.669 Å, with defocus ranging from -1.3 µm to -3.1 µm and a total fluence per
694 micrograph of 40 $e^-/Å^2$, fractionated into 40 frames.

695 Cryo-EM data processing

696 All cryo-EM data were processed using RELION-5.0 (Kimanius et al., 2023). Both datasets
697 were initially processed separately. Movies were corrected for motion using the RELION
698 implementation of MotionCor2, with 4x4 patches and dose-weighting. CTF parameters were
699 estimated using CTFFIND-4.1. Particle picking was done using Topaz with the general model
700 (Bepler et al., 2019), yielding 1,820,457 particles. 3D classification was performed on 4-fold
701 (dataset 1) or 5-fold (dataset 2) binned particles using a P-complex reference map (EMD-10140),
702 and 299,741 (dataset 1) or 599,123 (dataset 2) were selected and refined to 2.99 Å or 2.78 Å
703 resolution respectively. After Bayesian Polishing and CTF refinement (per-particle defocus,
704 anisotropic magnification, beam tilt, trefoil, and 4th order aberrations) the resolution improved to
705 2.67 Å or 2.32 Å respectively. To improve the general density quality, 3D classification without
706 alignment was performed with a soft mask around the whole complex with T=15. Particles with
707 good density, without selecting for Fyv6 occupancy, were selected (151,443 and 257,501 for
708 datasets 1 and 2) and refined to 2.66 Å or 2.27 Å respectively. The particles were then merged,
709 refined, and then refined for anisotropic magnification. The overall scaling factors from the
710 "anisotropic" magnification matrix was then used to calculate the corrected pixel size for dataset
711 1 as 0.94057 Å, keeping dataset 2 constant at 0.669 Å per pixel. Defocus values for dataset 1
712 were then scaled by the square of 0.94057 / 0.93, with an empirical constant correction of -10.06
713 Å (Wilkinson et al., 2019). Finally, another round of per-particle defocus refinement and
714 anisotropic magnification refinement was performed to reduce errors in defocus correction and
715 dataset scaling. The combined particles refined to 2.24 Å resolution. Resolution is reported using
716 the gold-standard Fourier Shell Correlation with 0.143 cutoff.

717 The refined particles after merging were subjected to 3D classification without alignment,
718 with a soft mask around the entire spliceosome, with T=15. The resulting four classes were used
719 to define States I, II and III. To improve the densities for the periphery of the spliceosome that
720 displayed local flexibility, focused refinements were used with Blush regularization in RELION-5
721 to reduce overfitting (Kimanius et al., 2023). The Prp22 density was improved using a soft-mask

722 just around the Prp22 helicase domain for refinement of particles from States I and II, yielding a
723 2.96 Å map. Densities for the U2 snRNP, NTC, U5 Sm ring, and Cwc22 N-terminal domain were
724 each improved first by 3D classification without alignment of particles from all three states,
725 selecting particles with strong density (72,869 for the U2 snRNP, 260,409 for the NTC, 113,561
726 for the U5 Sm ring, 201,984 for Cwc22-NTD), performing signal subtraction to remove density for
727 the rest of the spliceosome (recentering on the mask center of mass and re-boxing to 300 pixels,
728 or 192 pixels for Cwc22-NTD), and finally 3D refinement starting with 1.8 degree local angular
729 searches, giving 3.42 Å for the U2 snRNP, 3.72 Å for the NTC, 3.06 Å for the U5 Sm, and 3.57 Å
730 for Cwc22-NTD. In all cases, control refinements without Blush regularization did not produce
731 interpretable maps (**Supplemental Fig. S6).**

732 Model building

733 The model was built using Coot (Casañal et al., 2020) and ISOLDE (Croll, 2018) starting
734 with PDB 6EXN (Wilkinson et al., 2017) as an initial model for the core and PDB 7B9V (Wilkinson
735 et al., 2021) as an initial model for the periphery. The core was improved by manual fixing in Coot,
736 while the peripheral U2 snRNP and NTC were improved by applying torsion and distance
737 restraints to reference models produced by AlphaFold2. The model was refined using PHENIX
738 real_space_refine (Liebschner et al., 2019), just performing one macro-cycle. Figures were
739 generated using UCSF ChimeraX.

740 **Plasmid cloning**

741 Fyv6 plasmids were made by PCR amplification from gDNA of the *FYV6* coding sequence
742 plus ~250 nt upstream and downstream, restriction digest with NotI and SalI, and ligation into
743 pRS414 or pRS416. An N-terminal 1x FLAG tag was added onto Fyv6 in the plasmids by PCR
744 mutagenesis. Fyv6 truncations were cloned by Genewiz (Azenta Life Sciences) from pAAH1572.
745 Restriction digest and ligation were used to place Fyv6 constructs into the pRS413 backbone.

746 Syf1 plasmids were made by PCR amplification from gDNA of the SYF1 coding sequence
747 plus ~275 nt upstream and downstream, restriction digest, and ligation into pRS414 or pRS416.
748 Cef1 mutant plasmids, Prp22 I1133R mutant plasmid, Prp8 mutant plasmids, ACT1-CUP1
749 BP-3' SS distance reporters, and Syf1 truncation plasmids were prepared by PCR-based site
750 directed mutagenesis of pAAH1611, pAAH1042, pAAH1440, pAAH0470, and pAAH1625
751 respectively. All plasmids were fully sequenced to confirm their nucleotide sequence.

752 **Yeast strain creation**

753 The *DBR1* and *FYV6* genes were deleted by replacement with a nourseothricin resistance
754 cassette (NatMX4) or hygromycin resistance cassette (hphMX4), respectively, through
755 homologous recombination (see **Supplemental Table S7**; Goldstein and McCusker, 1999). The
756 *SYF1* and *CEF1* genes were deleted by replacement with a kanamycin resistance cassette
757 (KanMX) through homologous recombination in strains transformed with pRS416-Syf1 or
758 pRS316-Cef1 respectively. Gene deletion was confirmed by colony PCR and/or genomic DNA
759 extraction from the strains and PCR amplification of the corresponding genomic locus.

760 **RNA isolation**

761 Yeast were grown in YPD media until OD_{600} 0.5-0.8. For RNA-sequencing of temperature-
762 shifted samples, cultures were shifted to either 37°C or 16°C or remained at 30°C and grown for
763 1 hr. A 15 mL volume of culture was harvested via vacuum filtration with mixed cellulose ester
764 filter paper (Whatman, 47 mm diameter) in a Buchner funnel. Filter papers were separated into 5
765 mL tubes and flash frozen. Filters were stored at –80°C until RNA isolation. Filters were washed
766 with 1 mL TRIzol to collect cells. For all other experiments involving RNA isolation, 10 OD_{600} units
767 of OD_{600} 0.5-0.8 yeast were harvested via centrifugation.

768 Cell walls were disrupted by incubation with Zymolyase (50 U/mL, Zymo Research) in Y1
769 buffer (1 M sorbitol, 100 mM EDTA pH 8.0, 13 mM β-mercaptoethanol) (primer extension, RNA-
770 seq of non-temperature-shifted samples) or vortexing with silica disruption beads in TRIzol (RT-
771 PCR, RNA-seq of temperature-shifted samples). Total RNA was then isolated using TRIzol

772 reagent (Thermo Fisher Scientific) according to manufacturer's instructions. Samples were
773 cleaned using a 50 µg Monarch RNA Cleanup Kit (New England Biolabs) and treated with TURBO
774 DNase (Thermo Fisher Scientific) to remove residual contaminating DNA. For RNA-sequencing,
775 quality of RNA samples was assessed prior to library preparation by NanoDrop (concentration,
776 A_{260}/A_{280}, and A_{260}/A_{230}), Qubit (RNA High Sensitivity and RNA IQ), and TapeStation (RNA
777 ScreenTape Analysis). High quality samples showing minimal rRNA degradation with RIN >7 and
778 A260/A280 ratios of ~2.0 were selected for library preparation.

779 **Library preparation and RNA sequencing**

780 Library preparation was conducted by the University of Wisconsin-Madison Biotechnology
781 Center Gene Expression Center. mRNA was selected from total RNA samples through polyA
782 enrichment with the TruSeq Stranded mRNA kit (Illumina). Sequencing was performed with an
783 NovaSeq6000 sequencer (Illumina).

784 **Bioinformatic analysis of RNA-seq datasets**

785 FASTQC was used for quality control of reads pre- and post- trimming (Andrews, 2010).
786 Trimming of reads was accomplished using fastp (Chen et al., 2018) prior to mapping to the
787 SacCer3 genome (Ensembl, R64-1-1) with STAR (Dobin et al., 2013). All samples were aligned
788 with STAR in a first pass. Novel junctions from all samples (WT and *fyv6Δ*) were combined and
789 filtered for likely false-positive junctions (see Supplemental Methods). STAR was run in a second
790 pass with the additional input of the filtered set of novel junctions. Indexing of bam files was
791 accomplished with SAMtools (Li et al., 2009). Quantitation of read counts aligned to the SacCer3
792 transcriptome was accomplished with Salmon (Patro et al., 2017). Differential gene expression
793 analysis was conducted with DeSeq2 (Love et al., 2014). Junction reads within genes were
794 counted with featureCounts (Liao et al., 2014) and used to calculate fraction of Annotation Splicing
795 (FAnS) based on methods in Roy et al., 2023 (see Supplemental Methods). Canonical branch
796 points were used as defined in the Ares Intron Database (Grate and Ares, 2002). Differential
797 splicing analysis was conducted with SpliceWiz (Wong et al., 2024).

798 **Primer extension**

799 RNA was isolated using the protocol above. IR700 dye conjugated probes (Integrated DNA
800 Technologies) were used for primer extension with SuperScript III (Thermo Fisher) of the ACT1-
801 CUP1 reporters (2 pmol yAC6: /5IRD700/GGCACTCATGACCTTC) and U6 snRNA (0.4 pmol
802 yU6: /5IRD700/GAACTGCTGATCATGTCTG) (Carrocci et al., 2017; van der Feltz et al., 2021).
803 Primer extension products were visualized on a 7% (w/v) denaturing polyacrylamide gel run at 35
804 W for 80 min at RT. Gels were imaged with an Amersham Typhoon NIR laser scanner (Cytiva),
805 and band intensities were quantified with Image J (version 1.53v, 2022).

806 **RT-PCR**

807 Yeast cultures were inoculated from cultures grown to stationary phase overnight and
808 grown until OD_{600} = 0.7-0.9. RNA was isolated and depleted of contaminating DNA using the
809 MasterPure Yeast RNA Purification Kit (LGC Biosearch Technologies) protocol as previously
810 described (Carrocci et al., 2017) (RT-PCR shown in Fig. 4C) or using the RNA isolation protocol
811 above (all others).

812 RT-PCR reactions were set up using the Access RT-PCR system (Promega Corporation)
813 following the kit procedure with 100 ng of input RNA per 25 µl reaction. Primers to amplify *SUS1*
814 were SUS1-exon1 5'-TGGATACTGCGCAATTAAAGAGTC-3' and SUS1-exon3 5'-
815 TCATTGTGTATCTACAATCTCTTCAAG-3'. Reaction products were separated on 2% (w/v)
816 agarose-TBE gels and imaged using ethidium bromide fluorescence.

817 **Selection of *fyv6Δ* suppressors**

818 Strain yAAH3353 was previously described (Lipinski et al. 2023). Twenty single colonies
819 of yAAH3353 were selected from a YPD plate and used to inoculate 20 x 5mL YPD liquid culture.
820 Cultures were grown for 48 h at 30°C. A 1 mL volume of culture was spun down, resuspended in
821 200 µL YPD liquid medium, and spread on a YPD plate containing 40 mg/L adenine hemisulfate
822 (to prevent ade2 reversion). Duplicate plates for each overnight were placed in incubators at either
823 18°C or 37°C. Many colonies of various sizes appeared on each plate by 9 days for 37°C and 12

824 days for 18°C. Colonies were picked after that time and annotated first by growth temperature,
825 then by overnight number, and finally roughly by colony size with 01 generally being the largest
826 colony on a plate (ex: 370101 from a plate grown at 37°C inoculated from overnight 01 and the
827 largest colony selected from the plate). Picked colonies were grown overnight in 5mL YPD at 30°C
828 and frozen stocks were made. Anywhere from 0 to ~15 colonies were picked per plate, covering
829 the variety of colony sizes that arose.

830 **Sequencing of yeast genomic DNA**

831 Yeast were grown to saturated stationary phase in 5mL YPD and ~10 OD units were sent
832 as a frozen yeast pellet to Azenta or SeqCoast for genomic DNA extraction, library, preparation,
833 and sequencing with 30x/400 mbp coverage.

834 **Bioinformatic analysis of WGS data**

835 Azenta and SeqCoast utilized the SacCer3 genome (Ensembl, R64-1-1) for variant calling
836 and provided a list of >6,000 SNPs. Since the strain is not a perfect match for this reference, non-
837 unique SNPs were filtered from each dataset by taking the union of two sets with each set
838 obtained from colonies isolated on different plates (to reduce the chance of computationally
839 eliminating the same variant SNP). Filtering reduced the dataset to <100 unique variants per
840 colony. Few unique SNPs were within protein- or snRNA-coding genes. Of SNPs within protein-
841 coding regions, single amino acid changes were frequently found within splicing factors (see
842 **Supplemental Table S4**). Datasets were reexamined upon identification of suppressor mutations
843 for suppressor mutation duplication that were potentially filtered out during comparison of SNP
844 datasets.

845 **Yeast temperature growth assays**

846 Yeast were grown to stationary phase overnight in the appropriate liquid medium indicated
847 in the figure legends. The cultures were first diluted to OD_{600} 0.5, serially diluted 1:10, 1:100, and
848 1:1000, and stamped onto agar plates containing the appropriate growth medium. The plates

849 were incubated at 16°, 23°, 30°, and 37°C, and plates were imaged after the number of days
850 indicated in each figure.

851 **ACT1-CUP1 copper tolerance assays**

852 Yeast strains expressing ACT1-CUP1 reporters were grown to stationary phase in -Leu
853 DO media, diluted to OD_{600} = 0.5 in 10% (v/v) glycerol, and spotted onto -Leu DO plates containing
854 0 to 2.5 mM $CuSO_4$ (Lesser and Guthrie 1993; Carrocci et al., 2018). Plates were scored and
855 imaged after 48 h of growth at 30°C for WT strains and after 72 h of growth at 30°C for *fyv6Δ*
856 strains due to differential growth between strains.

857

858

859 **ACKNOWLEDGEMENTS**

860 We thank David Brow for his advice on the suppressor screen. We thank Justin Mabin for
861 his advice on RNA-sequencing data analysis. MEW is grateful to Feng Zhang for funding and
862 support, and to the labs of Kiyoshi Nagai and Kelly Nguyen for reagents and support. The authors
863 utilized the University of Wisconsin – Madison Biotechnology Center Gene Expression Center
864 (Research Resource Identifier – RRID:SCR_017757) for preparation of NGS libraries for RNA-
865 sequencing and the Biochemistry Computational Research Facility (BCRF) for analysis of RNA-
866 sequencing datasets. This work was supported by grants from the National Institutes of Health
867 (R35 GM136261 to AAH), NIH Biotechnology Training Program (T32 GM135066) and National
868 Science Foundation Graduate Research Fellowship Program (Grant No. DGE-1747503)
869 fellowships to KAS, a Helen Hay Whitney Postdoctoral Fellowship (to MEW). This study was
870 supported by the MRC Laboratory of Molecular Biology electron microscopy facility. We thank
871 Guillaume Chanfreau for advice and Florian Heyd and Tucker Carrocci for critical reading of the
872 manuscript.

873

874 **CONTRIBUTIONS**

875 AAH, KAS, KAL, and MEW conceptualized the project; MEW collected and analyzed the cryo-EM
876 data; KAL and NJZ prepared RNA for sequencing; KAL, NJZ, and AFG analyzed the RNA-
877 sequencing data; AAH, KAS, NJZ, and KAL created yeast strains; KAS, KAL, NJZ, and AFG
878 performed genetic and biochemical assays and analyzed data; KAS, KAL, MEW, and AAH wrote
879 the manuscript.
880

881 **DATA AND MATERIALS AVAILABILITY**

882 RNA-seq data has been uploaded to NCBI SRA with BioProject ID PRJNA1113593. The cryo-EM
883 maps will be deposited in the Electron Microscopy Data Bank and the atomic model to the Protein
884 Data Bank upon manuscript submission. Raw cryo-EM data will be available from EMPIAR.
885

886 **COMPETING INTEREST STATEMENT**

887 AAH is a member of the scientific advisory board and carrying out sponsored research for Remix
888 Therapeutics.
889

890 **REFERENCES**

891 Andrews, S. (2010). *FastQC: a quality control tool for high throughput sequence data* [Computer
892 software]. http://www.bioinformatics.babraham.ac.uk/projects/fastqc

893 Aronova, A., Bacíková, D., Crotti, L. B., Horowitz, D. S., & Schwer, B. (2007). Functional
894 interactions between Prp8, Prp18, Slu7, and U5 snRNA during the second step of pre-
895 mRNA splicing. *RNA*, *13*(9), 1437–1444. https://doi.org/10.1261/rna.572807

896 Bai, R., Yan, C., Wan, R., Lei, J., & Shi, Y. (2017). Structure of the Post-catalytic Spliceosome
897 from Saccharomyces cerevisiae. *Cell*, *171*(7), 1589-1598.e8.
898 https://doi.org/10.1016/j.cell.2017.10.038

899 Bepler, T., Morin, A., Rapp, M., Brasch, J., Shapiro, L., Noble, A. J., & Berger, B. (2019).
900 Positive-unlabeled convolutional neural networks for particle picking in cryo-electron
901 micrographs. *Nature Methods*, *16*(11), Article 11. https://doi.org/10.1038/s41592-019-
902 0575-8

903 Brow, D. A. (2019). An Allosteric Network for Spliceosome Activation Revealed by High-
904 Throughput Suppressor Analysis in Saccharomyces cerevisiae. *Genetics*, *212*(1), 111–
905 124. https://doi.org/10.1534/genetics.119.301922

906 Brys, A., & Schwer, B. (1996). Requirement for SLU7 in yeast pre-mRNA splicing is dictated by
907 the distance between the branchpoint and the 3' splice site. *RNA*, *2*(7), 707–717.

908 Carrocci, T. J., Paulson, J. C., & Hoskins, A. A. (2018). Functional analysis of Hsh155/SF3b1
909 interactions with the U2 snRNA/branch site duplex. *RNA*, *24*(8), 1028–1040.
910 https://doi.org/10.1261/rna.065664.118

911 Carrocci, T. J., Zoerner, D. M., Paulson, J. C., & Hoskins, A. A. (2017). SF3b1 mutations
912 associated with myelodysplastic syndromes alter the fidelity of branchsite selection in
913 yeast. *Nucleic Acids Research*, *45*(8), 4837–4852. https://doi.org/10.1093/nar/gkw1349

914 Casañal, A., Lohkamp, B., & Emsley, P. (2020). Current developments in Coot for
915 macromolecular model building of Electron Cryo-microscopy and Crystallographic Data.
916 *Protein Science*, *29*(4), 1055–1064. https://doi.org/10.1002/pro.3791

917 Chen, C.-H., Tsai, W.-Y., Chen, H.-R., Wang, C.-H., & Cheng, S.-C. (2001). Identification and
918 Characterization of Two Novel Components of The Prp19p-associated Complex, Ntc30p
919 and Ntc20p *. *Journal of Biological Chemistry*, *276*(1), 488–494.
920 https://doi.org/10.1074/jbc.M006958200

921 Chen, S., Zhou, Y., Chen, Y., & Gu, J. (2018). fastp: An ultra-fast all-in-one FASTQ
922 preprocessor. *Bioinformatics*, *34*(17), i884–i890.
923 https://doi.org/10.1093/bioinformatics/bty560

924 Chiang, T.-W., & Cheng, S.-C. (2013). A Weak Spliceosome-Binding Domain of Yju2 Functions
925 in the First Step and Bypasses Prp16 in the Second Step of Splicing. *Molecular and*
926 *Cellular Biology*, *33*(9), 1746–1755. https://doi.org/10.1128/MCB.00035-13

927 Chua, K., & Reed, R. (1999). The RNA splicing factor hSlu7 is required for correct 3′ splice-site
928 choice. *Nature*, *402*(6758), 207–210. https://doi.org/10.1038/46086

929 Chung, C.-S., Wai, H. L., Kao, C.-Y., & Cheng, S.-C. (2023). An ATP-independent role for Prp16
930 in promoting aberrant splicing. *Nucleic Acids Research*, *51*(20), 10815–10828.
931 https://doi.org/10.1093/nar/gkad861

932 Chung, S., McLean, M. R., & Rymond, B. C. (1999). Yeast ortholog of the Drosophila crooked
933 neck protein promotes spliceosome assembly through stable U4/U6.U5 snRNP addition.
934 *RNA*, *5*(8), 1042–1054.

935 Company, M., Arenas, J., & Abelson, J. (1991). Requirement of the RNA helicase-like protein
936 PRP22 for release of messenger RNA from spliceosomes. *Nature*, *349*(6309), 487–493.
937 https://doi.org/10.1038/349487a0

938 Corvelo, A., Hallegger, M., Smith, C. W. J., & Eyras, E. (2010). Genome-Wide Association
939 between Branch Point Properties and Alternative Splicing. *PLOS Computational Biology*,
940 *6*(11), e1001016. https://doi.org/10.1371/journal.pcbi.1001016

941 Croll, T. I. (2018). ISOLDE: A physically realistic environment for model building into low-
942 resolution electron-density maps. *Acta Crystallographica Section D: Structural Biology*,
943 *74*(6), 519–530. https://doi.org/10.1107/S2059798318002425

944 Crotti, L. B., Bačíková, D., & Horowitz, D. S. (2007). The Prp18 protein stabilizes the interaction
945 of both exons with the U5 snRNA during the second step of pre-mRNA splicing. *Genes &*
946 *Development*, *21*(10), 1204–1216. https://doi.org/10.1101/gad.1538207

947 Dobin, A., Davis, C. A., Schlesinger, F., Drenkow, J., Zaleski, C., Jha, S., Batut, P., Chaisson,
948 M., & Gingeras, T. R. (2013). STAR: Ultrafast universal RNA-seq aligner. *Bioinformatics*,
949 *29*(1), 15–21. https://doi.org/10.1093/bioinformatics/bts635

950 Felisberto-Rodrigues, C., Thomas, J. C., McAndrew, C., Le Bihan, Y.-V., Burke, R., Workman,
951 P., & van Montfort, R. L. M. (2019). Structural and functional characterisation of human

RNA helicase DHX8 provides insights into the mechanism of RNA-stimulated ADP release. *Biochemical Journal*, *476*(18), 2521–2543. https://doi.org/10.1042/BCJ20190383

Feltz, C. van der, Nikolai, B., Schneider, C., Paulson, J. C., Fu, X., & Hoskins, A. A. (2021). Saccharomyces cerevisiae Ecm2 modulates the catalytic steps of pre-mRNA splicing. *RNA*, *27*(5), 591–603. https://doi.org/10.1261/rna.077727.120

Fica, S. M., & Nagai, K. (2017). Cryo-electron microscopy snapshots of the spliceosome: Structural insights into a dynamic ribonucleoprotein machine. *Nature Structural & Molecular Biology*, *24*(10), Article 10. https://doi.org/10.1038/nsmb.3463

Fica, S. M., Oubridge, C., Wilkinson, M. E., Newman, A. J., & Nagai, K. (2019). A human postcatalytic spliceosome structure reveals essential roles of metazoan factors for exon ligation. *Science*, *363*(6428), 710–714. https://doi.org/10.1126/science.aaw5569

Frank, D., & Guthrie, C. (1992). An essential splicing factor, SLU7, mediates 3' splice site choice in yeast. *Genes & Development*, *6*(11), 2112–2124. https://doi.org/10.1101/gad.6.11.2112

Galej, W. P., Oubridge, C., Newman, A. J., & Nagai, K. (2013). Crystal structure of Prp8 reveals active site cavity of the spliceosome. *Nature*, *493*(7434), 638–643. https://doi.org/10.1038/nature11843

Gautam, A., Grainger, R. J., Vilardell, J., Barrass, J. D., & Beggs, J. D. (2015). Cwc21p promotes the second step conformation of the spliceosome and modulates 3′ splice site selection. *Nucleic Acids Research*, *43*(6), 3309–3317. https://doi.org/10.1093/nar/gkv159

Goldstein, A. L., & McCusker, J. H. (1999). Three new dominant drug resistance cassettes for gene disruption in Saccharomyces cerevisiae. *Yeast*, *15*(14), 1541–1553. https://doi.org/10.1002/(SICI)1097-0061(199910)15:14<1541::AID-YEA476>3.0.CO;2-K

Gooding, C., Clark, F., Wollerton, M. C., Grellscheid, S.-N., Groom, H., & Smith, C. W. (2006). A class of human exons with predicted distant branch points revealed by analysis of AG dinucleotide exclusion zones. *Genome Biology*, *7*(1), R1. https://doi.org/10.1186/gb-2006-7-1-r1

Grate, L., & Ares, M. (2002). Searching yeast intron data at ares lab web site. In C. Guthrie & G. R. Fink (Eds.), *Methods in Enzymology* (Vol. 350, pp. 380–392). Academic Press. https://doi.org/10.1016/S0076-6879(02)50975-7

Kawashima, T., Douglass, S., Gabunilas, J., Pellegrini, M., & Chanfreau, G. F. (2014). Widespread Use of Non-productive Alternative Splice Sites in Saccharomyces cerevisiae. *PLOS Genetics*, *10*(4), e1004249. https://doi.org/10.1371/journal.pgen.1004249

Kimanius, D., Jamali, K., Wilkinson, M. E., Lövestam, S., Velazhahan, V., Nakane, T., & Scheres, S. H. W. (2023). *Data-driven regularisation lowers the size barrier of cryo-EM structure determination* (p. 2023.10.23.563586). bioRxiv. https://doi.org/10.1101/2023.10.23.563586

Koodathingal, P., Novak, T., Piccirilli, J. A., & Staley, J. P. (2010). The DEAH Box ATPases Prp16 and Prp43 Cooperate to Proofread 5′ Splice Site Cleavage during Pre-mRNA Splicing. *Molecular Cell*, *39*(3), 385–395. https://doi.org/10.1016/j.molcel.2010.07.014

Kuhn, A. N., & Brow, D. A. (2000). Suppressors of a Cold-Sensitive Mutation in Yeast U4 RNA Define Five Domains in the Splicing Factor Prp8 That Influence Spliceosome Activation. *Genetics*, *155*(4), 1667–1682. https://doi.org/10.1093/genetics/155.4.1667

997 Kuhn, A. N., Li, Z., & Brow, D. A. (1999). Splicing Factor Prp8 Governs U4/U6 RNA Unwinding
998 during Activation of the Spliceosome. *Molecular Cell*, *3*(1), 65–75.
999 https://doi.org/10.1016/S1097-2765(00)80175-6

1000 Lesser, C. F., & Guthrie, C. (1993). Mutational analysis of pre-mRNA splicing in Saccharomyces
1001 cerevisiae using a sensitive new reporter gene, CUP1. *Genetics*, *133*(4), 851–863.
1002 https://doi.org/10.1093/genetics/133.4.851

1003 Li, H., Handsaker, B., Wysoker, A., Fennell, T., Ruan, J., Homer, N., Marth, G., Abecasis, G.,
1004 Durbin, R., & 1000 Genome Project Data Processing Subgroup. (2009). The Sequence
1005 Alignment/Map format and SAMtools. *Bioinformatics*, *25*(16), 2078–2079.
1006 https://doi.org/10.1093/bioinformatics/btp352

1007 Liang, W.-W., & Cheng, S.-C. (2015). A novel mechanism for Prp5 function in prespliceosome
1008 formation and proofreading the branch site sequence. *Genes & Development*, *29*(1), 81–
1009 93. https://doi.org/10.1101/gad.253708.114

1010 Liao, Y., Smyth, G. K., & Shi, W. (2014). featureCounts: An efficient general purpose program for
1011 assigning sequence reads to genomic features. *Bioinformatics*, *30*(7), 923–930.
1012 https://doi.org/10.1093/bioinformatics/btt656

1013 Liebschner, D., Afonine, P. V., Baker, M. L., Bunkóczi, G., Chen, V. B., Croll, T. I., Hintze, B.,
1014 Hung, L. W., Jain, S., McCoy, A. J., Moriarty, N. W., Oeffner, R. D., Poon, B. K., Prisant,
1015 M. G., Read, R. J., Richardson, J. S., Richardson, D. C., Sammito, M. D., Sobolev, O. V.,
1016 … Adams, P. D. (2019). Macromolecular structure determination using X-rays, neutrons
1017 and electrons: Recent developments in Phenix. *Acta Crystallographica. Section D,*
1018 *Structural Biology*, *75*(Pt 10), 861–877. https://doi.org/10.1107/S2059798319011471

1019 Lin, R. J., Newman, A. J., Cheng, S. C., & Abelson, J. (1985). Yeast mRNA splicing in vitro.
1020 *Journal of Biological Chemistry*, *260*(27), 14780–14792. https://doi.org/10.1016/S0021-
1021 9258(17)38641-6

1022 Lipinski, K. A., Senn, K. A., Zeps, N. J., & Hoskins, A. A. (2023). Biochemical and Genetic
1023 Evidence Supports Fyv6 as a Second-Step Splicing Factor in Saccharomyces
1024 cerevisiae. *RNA*, rna.079607.123. https://doi.org/10.1261/rna.079607.123

1025 Liu, L., Query, C. C., & Konarska, M. M. (2007). Opposing classes of prp8 alleles modulate the
1026 transition between the catalytic steps of pre-mRNA splicing. *Nature Structural &*
1027 *Molecular Biology*, *14*(6), Article 6. https://doi.org/10.1038/nsmb1240

1028 Liu, S., Li, X., Zhang, L., Jiang, J., Hill, R. C., Cui, Y., Hansen, K. C., Zhou, Z. H., & Zhao, R.
1029 (2017). Structure of the yeast spliceosomal postcatalytic P complex. *Science*, *358*(6368),
1030 Article 6368. https://doi.org/10.1126/science.aar3462

1031 Love, M. I., Huber, W., & Anders, S. (2014). Moderated estimation of fold change and dispersion
1032 for RNA-seq data with DESeq2. *Genome Biology*, *15*(12), 550.
1033 https://doi.org/10.1186/s13059-014-0550-8

1034 Mayas, R. M., Maita, H., & Staley, J. P. (2006). Exon ligation is proofread by the DExD/H-box
1035 ATPase Prp22p. *Nature Structural & Molecular Biology*, *13*(6), Article 6.
1036 https://doi.org/10.1038/nsmb1093

1037 McPheeters, D. S., & Abelson, J. (1992). Mutational analysis of the yeast U2 snRNA suggests a
1038 structural similarity to the catalytic core of group I introns. *Cell*, *71*(5), 819–831.
1039 https://doi.org/10.1016/0092-8674(92)90557-s

1040 Mendoza-Ochoa, G. I., Barrass, J. D., Maudlin, I. E., & Beggs, J. D. (2019). Blocking late stages
1041 of splicing quickly limits pre-spliceosome assembly in vivo. *RNA Biology*, *16*(12), 1775–
1042 1784. https://doi.org/10.1080/15476286.2019.1657788

1043 Montemayor, E. J., Curran, E. C., Liao, H. H., Andrews, K. L., Treba, C. N., Butcher, S. E., &
1044 Brow, D. A. (2014). Core structure of the U6 small nuclear ribonucleoprotein at 1.7-Å
1045 resolution. *Nature Structural & Molecular Biology*, *21*(6), Article 6.
1046 https://doi.org/10.1038/nsmb.2832

1047 Mumberg, D., Müller, R., & Funk, M. (1995). Yeast vectors for the controlled expression of
1048 heterologous proteins in different genetic backgrounds. *Gene*, *156*(1), 119–122.
1049 https://doi.org/10.1016/0378-1119(95)00037-7

1050 Munding, E. M., Shiue, L., Katzman, S., Donohue, J. P., & Ares, M. (2013). Competition
1051 between Pre-mRNAs for the Splicing Machinery Drives Global Regulation of Splicing.
1052 *Molecular Cell*, *51*(3), 338–348. https://doi.org/10.1016/j.molcel.2013.06.012

1053 Nguyen Ba, A. N., Pogoutse, A., Provart, N., & Moses, A. M. (2009). NLStradamus: A simple
1054 Hidden Markov Model for nuclear localization signal prediction. *BMC Bioinformatics*,
1055 *10*(1), 202. https://doi.org/10.1186/1471-2105-10-202

1056 Patro, R., Duggal, G., Love, M. I., Irizarry, R. A., & Kingsford, C. (2017). Salmon provides fast
1057 and bias-aware quantification of transcript expression. *Nature Methods*, *14*(4), 417–419.
1058 https://doi.org/10.1038/nmeth.4197

1059 Perriman, R., Barta, I., Voeltz, G. K., Abelson, J., & Ares, M. (2003). ATP requirement for Prp5p
1060 function is determined by Cus2p and the structure of U2 small nuclear RNA.
1061 *Proceedings of the National Academy of Sciences*, *100*(24), 13857–13862.
1062 https://doi.org/10.1073/pnas.2036312100

1063 Plaschka, C., Newman, A. J., & Nagai, K. (2019). Structural Basis of Nuclear pre-mRNA
1064 Splicing: Lessons from Yeast. *Cold Spring Harbor Perspectives in Biology*, *11*(5),
1065 a032391. https://doi.org/10.1101/cshperspect.a032391

1066 Query, C. C., & Konarska, M. M. (2004). Suppression of Multiple Substrate Mutations by
1067 Spliceosomal prp8 Alleles Suggests Functional Correlations with Ribosomal Ambiguity
1068 Mutants. *Molecular Cell*, *14*(3), 343–354. https://doi.org/10.1016/S1097-2765(04)00217-
1069 5

1070 Query, C. C., & Konarska, M. M. (2012). CEF1/CDC5 alleles modulate transitions between
1071 catalytic conformations of the spliceosome. *RNA*, *18*(5), 1001–1013.
1072 https://doi.org/10.1261/rna.029421.111

1073 Roy, K. R., Gabunilas, J., Neutel, D., Ai, M., Yeh, Z., Samson, J., Lyu, G., & Chanfreau, G. F.
1074 (2023). Splicing factor Prp18p promotes genome-wide fidelity of consensus 3′-splice
1075 sites. *Nucleic Acids Research*, gkad968. https://doi.org/10.1093/nar/gkad968

1076 Sayani, S., Janis, M., Lee, C. Y., Toesca, I., & Chanfreau, G. F. (2008). Widespread Impact of
1077 Nonsense-Mediated mRNA Decay on the Yeast Intronome. *Molecular Cell*, *31*(3), 360–
1078 370. https://doi.org/10.1016/j.molcel.2008.07.005

1079 Schwer, B. (2008). A Conformational Rearrangement in the Spliceosome Sets the Stage for
1080 Prp22-Dependent mRNA Release. *Molecular Cell*, *30*(6), Article 6.
1081 https://doi.org/10.1016/j.molcel.2008.05.003

1082 Schwer, B., & Gross, C. H. (1998). Prp22, a DExH-box RNA helicase, plays two distinct roles in
1083 yeast pre-mRNA splicing. *The EMBO Journal*, *17*(7), 2086–2094.
1084 https://doi.org/10.1093/emboj/17.7.2086

Schwer, B., & Guthrie, C. (1992). A conformational rearrangement in the spliceosome is dependent on PRP16 and ATP hydrolysis. *The EMBO Journal*, *11*(13), 5033–5039. https://doi.org/10.1002/j.1460-2075.1992.tb05610.x

Schwer, B., & Meszaros, T. (2000). RNA helicase dynamics in pre-mRNA splicing. *The EMBO Journal*, *19*(23), 6582–6591. https://doi.org/10.1093/emboj/19.23.6582

Semlow, D. R., Blanco, M. R., Walter, N. G., & Staley, J. P. (2016). Spliceosomal DEAH-Box ATPases Remodel Pre-mRNA to Activate Alternative Splice Sites. *Cell*, *164*(5), Article 5. https://doi.org/10.1016/j.cell.2016.01.025

Semlow, D. R., & Staley, J. P. (2012). Staying on message: Ensuring fidelity in pre-mRNA splicing. *Trends in Biochemical Sciences*, *37*(7), 263–273. https://doi.org/10.1016/j.tibs.2012.04.001

Siatecka, M., Reyes, J. L., & Konarska, M. M. (1999). Functional interactions of Prp8 with both splice sites at the spliceosomal catalytic center. *Genes & Development*, *13*(15), 1983–1993.

Sikorski, R. S., & Boeke, J. D. (1991). In Vitro Mutagenesis and Plasmid Shuffling: From Cloned Gene to Mutant Yeast. *Methods in Enzymology*, *194*(C), 302–318. https://doi.org/10.1016/0076-6879(91)94023-6

Strittmatter, L. M., Capitanchik, C., Newman, A. J., Hallegger, M., Norman, C. M., Fica, S. M., Oubridge, C., Luscombe, N. M., Ule, J., & Nagai, K. (2021). psiCLIP reveals dynamic RNA binding by DEAH-box helicases before and after exon ligation. *Nature Communications*, *12*(1), 1488. https://doi.org/10.1038/s41467-021-21745-9

Talkish, J., Igel, H., Hunter, O., Horner, S. W., Jeffery, N. N., Leach, J. R., Jenkins, J. L., Kielkopf, C. L., & Ares, M. (2019). Cus2 enforces the first ATP-dependent step of splicing by binding to yeast SF3b1 through a UHM–ULM interaction. *RNA*, *25*(8), 1020–1037. https://doi.org/10.1261/rna.070649.119

Townsend, C., Leelaram, M. N., Agafonov, D. E., Dybkov, O., Will, C. L., Bertram, K., Urlaub, H., Kastner, B., Stark, H., & Lührmann, R. (2020). Mechanism of protein-guided folding of the active site U2/U6 RNA during spliceosome activation. *Science*, *370*(6523), eabc3753. https://doi.org/10.1126/science.abc3753

Treco, D. A., & Lundblad, V. (1993). Preparation of Yeast Media. *Current Protocols in Molecular Biology*, *23*(1), 13.1.1-13.1.7. https://doi.org/10.1002/0471142727.mb1301s23

Wan, R., Yan, C., Bai, R., Lei, J., & Shi, Y. (2017). Structure of an Intron Lariat Spliceosome from Saccharomyces cerevisiae. *Cell*, *171*(1), 120-132.e12. https://doi.org/10.1016/j.cell.2017.08.029

Wilkinson, M. E., Fica, S. M., Galej, W. P., & Nagai, K. (2021). Structural basis for conformational equilibrium of the catalytic spliceosome. *Molecular Cell*. https://doi.org/10.1016/j.molcel.2021.02.021

Wilkinson, M. E., Fica, S. M., Galej, W. P., Norman, C. M., Newman, A. J., & Nagai, K. (2017). Postcatalytic spliceosome structure reveals mechanism of 3′–splice site selection. *Science*, *358*(6368), 1283–1288. https://doi.org/10.1126/science.aar3729

Wilkinson, M. E., Kumar, A., & Casañal, A. (2019). Methods for merging data sets in electron cryo-microscopy. *Acta Crystallographica Section D: Structural Biology*, *75*(9), 782–791. https://doi.org/10.1107/S2059798319010519

1128 Wong, A. C. H., Wong, J. J.-L., Rasko, J. E. J., & Schmitz, U. (2024). SpliceWiz: Interactive
1129 analysis and visualization of alternative splicing in R. *Briefings in Bioinformatics*, *25*(1),
1130 bbad468. https://doi.org/10.1093/bib/bbad468

1131 Wu, T., Ruan, K., & Liu, W. (1996). A Fluorescence-Labeling Method for Sequencing Small RNA
1132 on Polyacrylamide Gel. *Nucleic Acids Research*, *24*(17), 3472–3473.
1133 https://doi.org/10.1093/nar/24.17.3472

1134 Xu, Y.-Z., & Query, C. C. (2007). Competition between the ATPase Prp5 and Branch Region-U2
1135 snRNA Pairing Modulates the Fidelity of Spliceosome Assembly. *Molecular Cell*, *28*(5),
1136 838–849. https://doi.org/10.1016/j.molcel.2007.09.022

1137 Yan, D., Perriman, R., Igel, H., Howe, K. J., Neville, M., & Ares Jr., M. (1998). CUS2, a Yeast
1138 Homolog of Human Tat-SF1, Rescues Function of Misfolded U2 through an Unusual
1139 RNA Recognition Motif. *Molecular and Cellular Biology*, *18*(9), 5000–5009.
1140 https://doi.org/10.1128/MCB.18.9.5000

1141 Zhan, X., Lu, Y., Zhang, X., Yan, C., & Shi, Y. (2022). Mechanism of exon ligation by human
1142 spliceosome. *Molecular Cell*, *82*(15), Article 15.
1143 https://doi.org/10.1016/j.molcel.2022.05.021

1144 Zhang, X., & Schwer, B. (1997). Functional and physical interaction between the yeast splicing
1145 factors Slu7 and Prp18. *Nucleic Acids Research*, *25*(11), 2146–2152.
1146 https://doi.org/10.1093/nar/25.11.2146

1147 Zhang, X., Zhan, X., Yan, C., Zhang, W., Liu, D., Lei, J., & Shi, Y. (2019). Structures of the
1148 human spliceosomes before and after release of the ligated exon. *Cell Research*, *29*(4),
1149 Article 4. https://doi.org/10.1038/s41422-019-0143-x

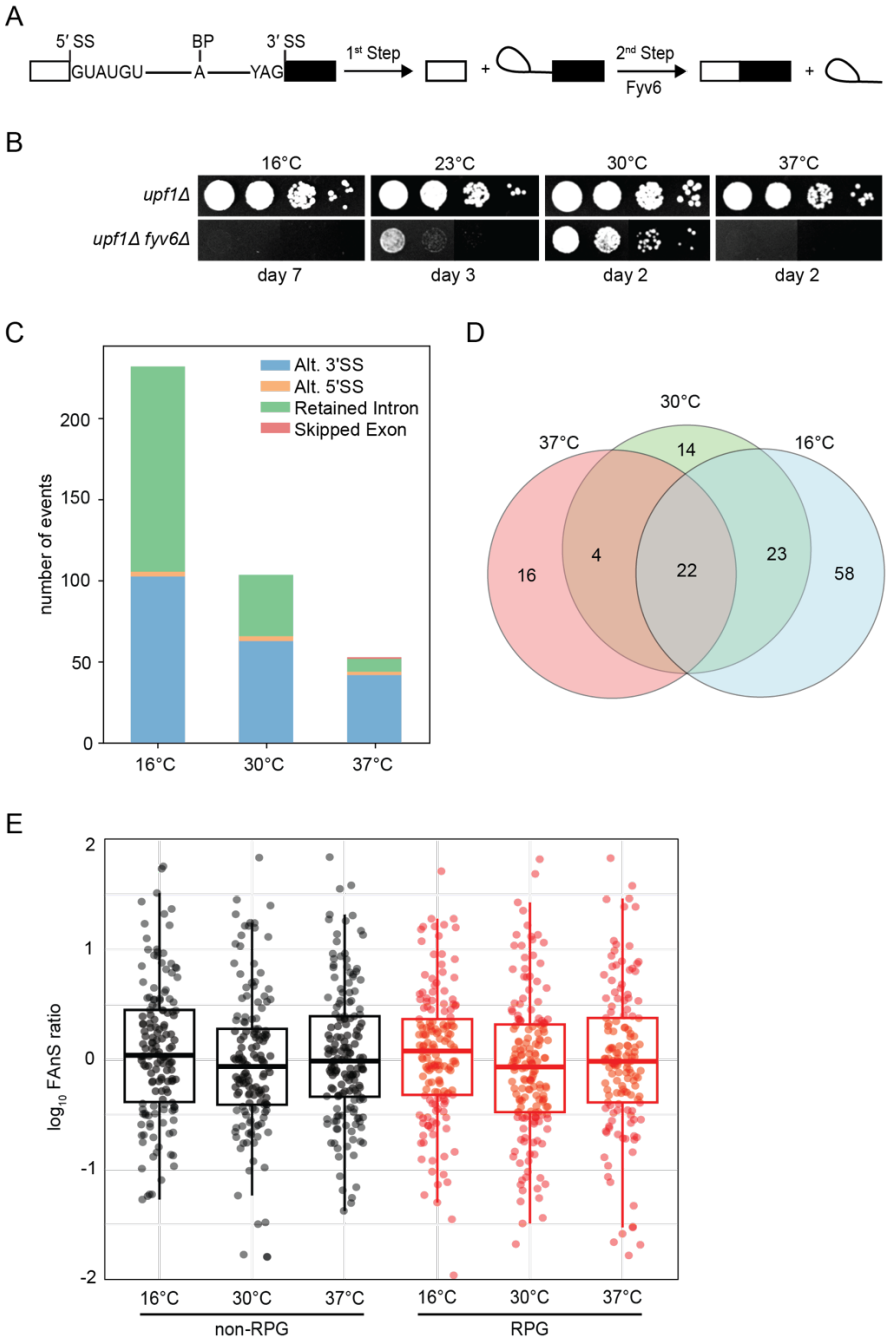

Figure 1. Widespread splicing changes due to loss of Fyv6. A) Pre-mRNA splicing reaction steps and products. **B)** Growth of *upf1Δ* and *fyv6Δupf1Δ* yeast at 16, 23, 30, and 37°C. Images were taken on the indicated days. **C)** Number of alternative splicing events observed in a *fyv6Δupf1Δ* strain relative to a strain containing FYV6 after a temperature shift to 16, 30, and 37°C. **D)** Venn diagram of shared alternative splicing events at 16 (blue), 30 (green), and 37°C (red). **E)** Box plots of the $\log_{10}$ of the ratios of *fyv6Δ upf1Δ* to WT (*upf1Δ*) FAnS for RPGs (red) and non-RPGs (black).

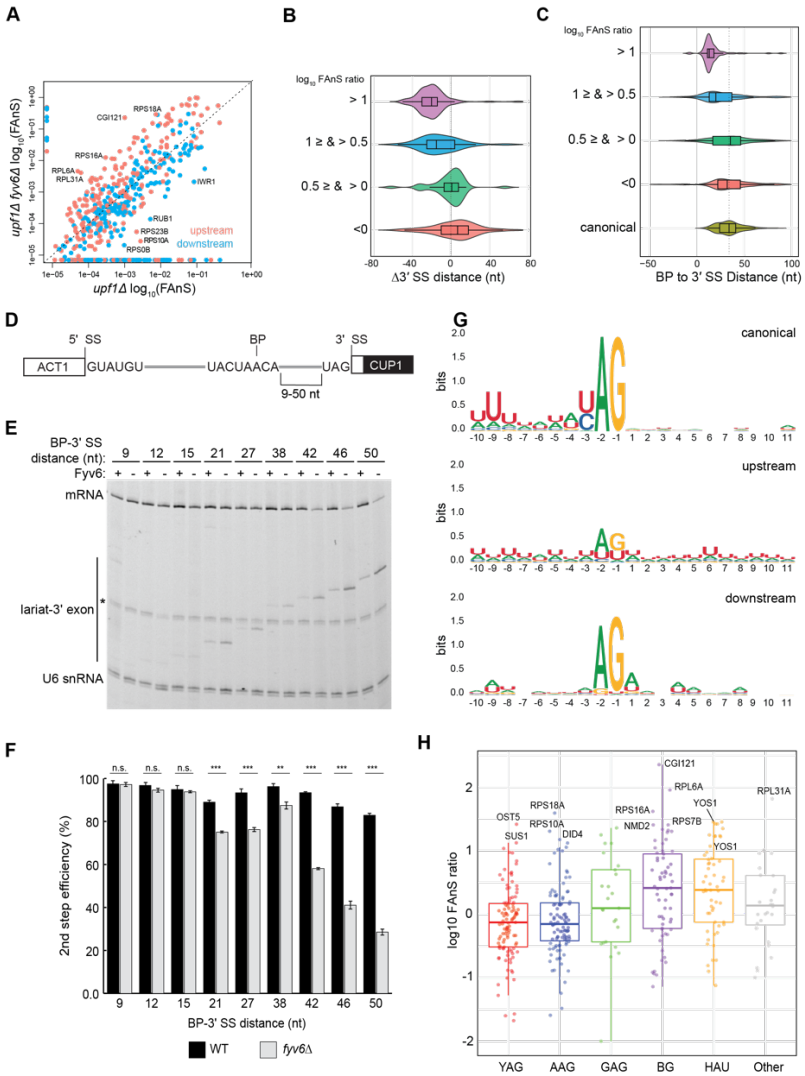

Figure 2: Loss of Fyv6 activates BP proximal, non-consensus 3' SS. A) Plot of the $\log_{10}$ of FAnS values for changes in alternative 3' SS usage in *fyv6Δ upf1Δ* and *upf1Δ* strains. Points are colored based on whether they are upstream (pink) or downstream (blue) to the canonical 3' SS. **B)** Violin plots of the ratios of *fyv6Δupf1Δ* to the *upf1Δ* FAnS values based on the distances between the alternative and canonical 3' SS. FAnS ratios >0 are indicative of the site being upregulated in *fyv6Δ*. **C)** Violin plots of the ratios of *fyv6Δupf1Δ* to the *upf1Δ* FAnS values based on the distances between the alternative 3' SS and the annotated BP. FAnS ratios >0 are indicative of the site being upregulated in *fyv6Δ*. **D)** Diagram of ACT1-CUP1 reporter showing BP-3' SS distances. **E)** Representative primer extension analysis of RNA products generated from splicing of the ACT1-CUP1 reporter in the presence (WT) or absence of Fyv6 (*fyv6Δ*). Bands for fully spliced mRNA and lariat intermediate are indicated. U6 snRNA was detected as a loading control. The * indicates an unknown product present in every lane. **F)** Quantification of the primer extension results from *N*=3 replicates represented by the ratio of band intensities for mRNA/(mRNA+lariat intermediate). Bars represent the average ratio of the replicates ±SD. Means between WT and *fyv6Δ* groups for each reporter were compared with an unpaired Welch's two-tailed t-test. Significance is indicated: n.s. no significance; ** $p<0.01$; *** $p<0.001$. **G)** Sequence logos of alternative 3' SS with FAnS > 0 sorted by either upstream or downstream of the canonical 3' SS compared against the canonical 3' SS for genes with FanS > 0. **H)** The $\log_{10}$ of the FAnS ratio for alternative 3' SS sorted by the sequences of the 3' SS.

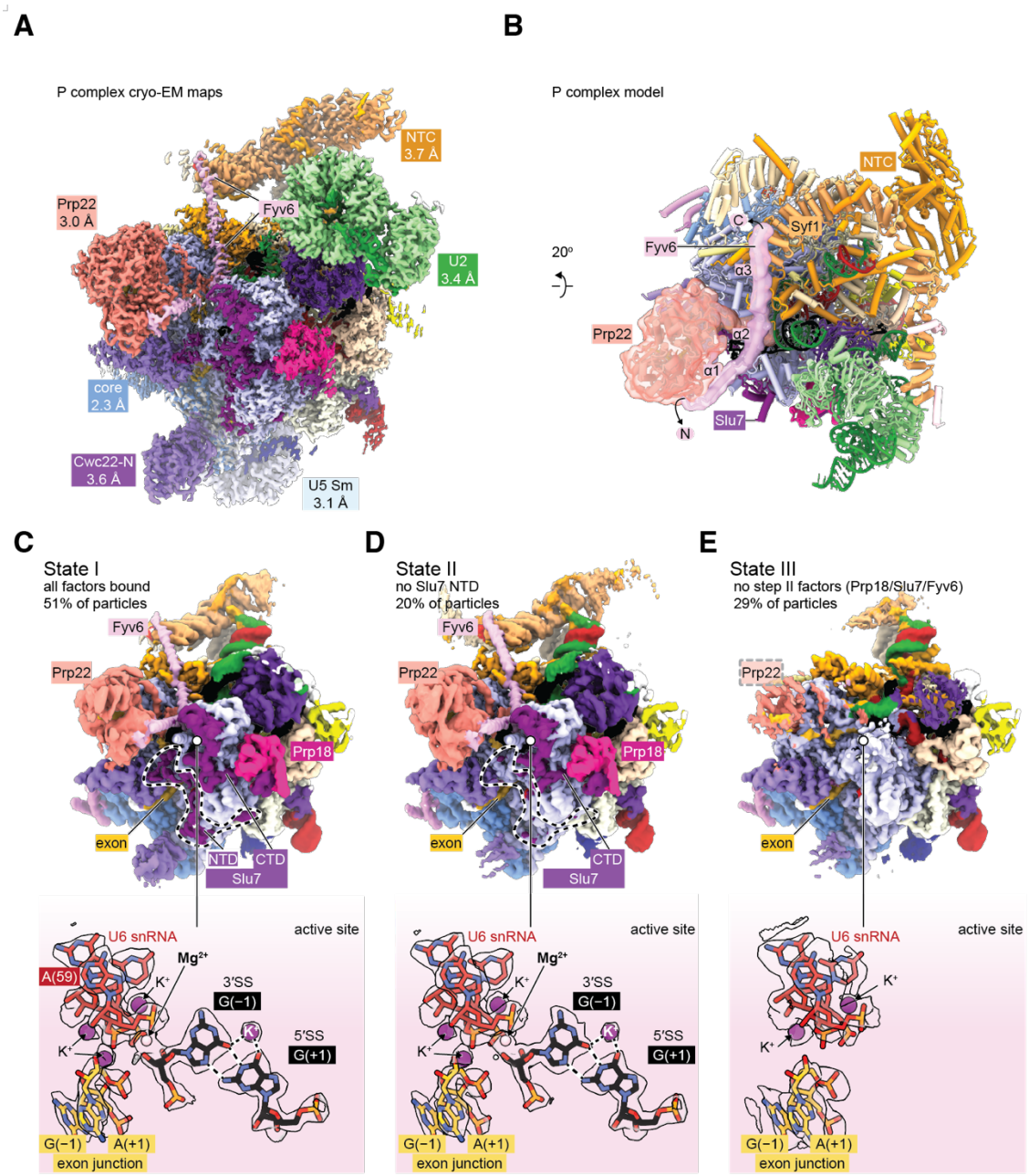

Figure 3. Cryo-EM structure of the yeast P complex spliceosome at 2.3 Å resolution. A) A composite density map for P complex showing focused refinements of the Prp22, NTC, U2 snRNP, U5 Sm ring, and Cwc22 N-terminal domain regions. **B)** Overall model for the P complex spliceosome. **C)** Cryo-EM density for state I of P complex (above, low-pass filtered) and for the active site and 3' SS (below, sharpened). **D,E**) As for **C)** but for states II (**D**) and III (**E**).

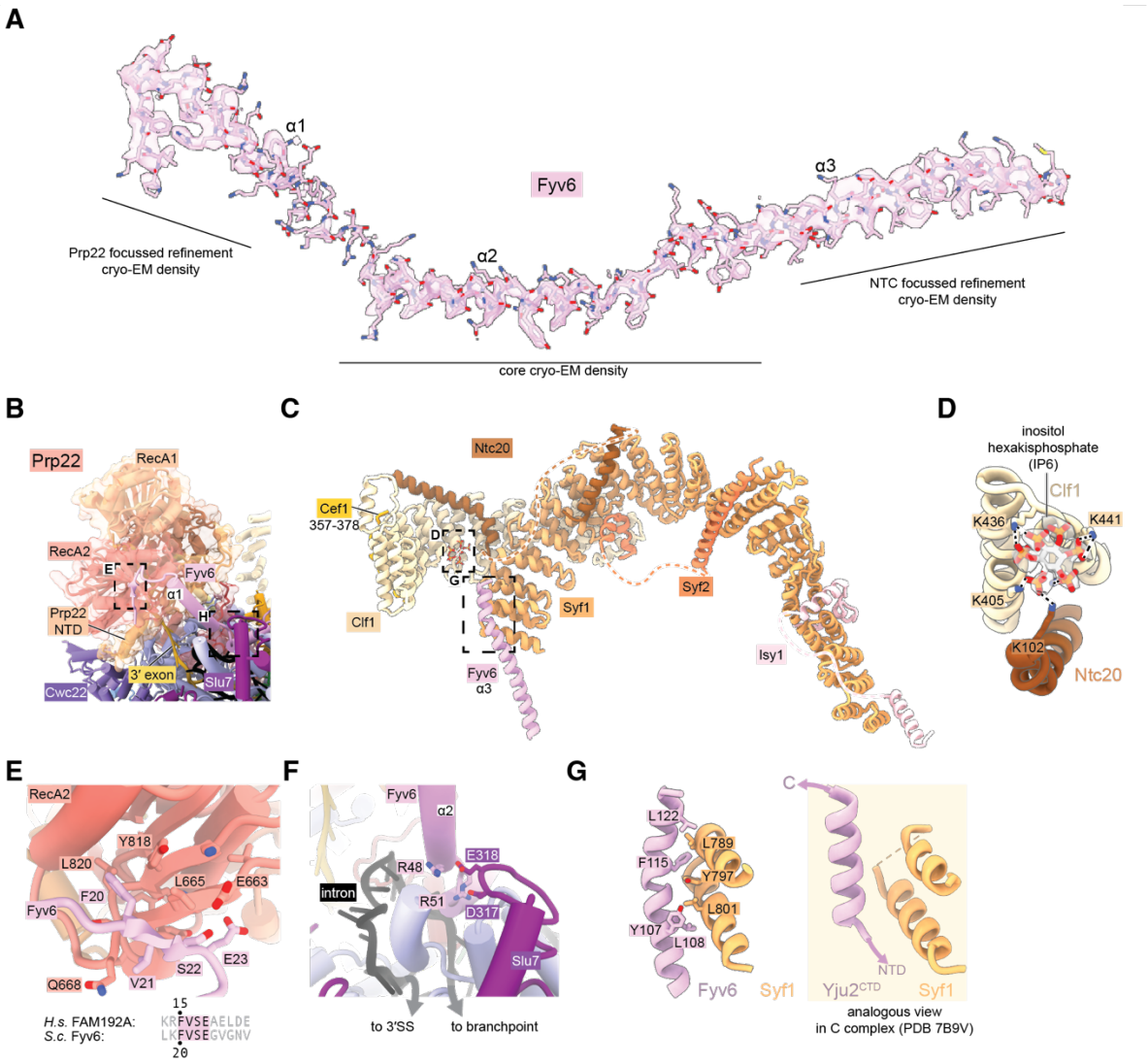

Figure 4. Fyv6 and its interactors in the P complex cryo-EM structure. A) Cryo-EM density segmented around Fyv6. **B)** Structure of Prp22. **C)** Structure of the NTC within P complex. **D)** IP_6 site and cryo-EM density in NTC. **E)** Interaction of the hook domain of Fyv6 with the Prp22 RecA2 domain. **F)** Interaction of Fyv6 with Slu7 and the region of the intron between the BP and 3' SS. **G)** Interaction of Fyv6 with Syf1 and an analogous view of the interaction of Syf1 with Yju2 in C complex (Wilkinson et al., 2021).

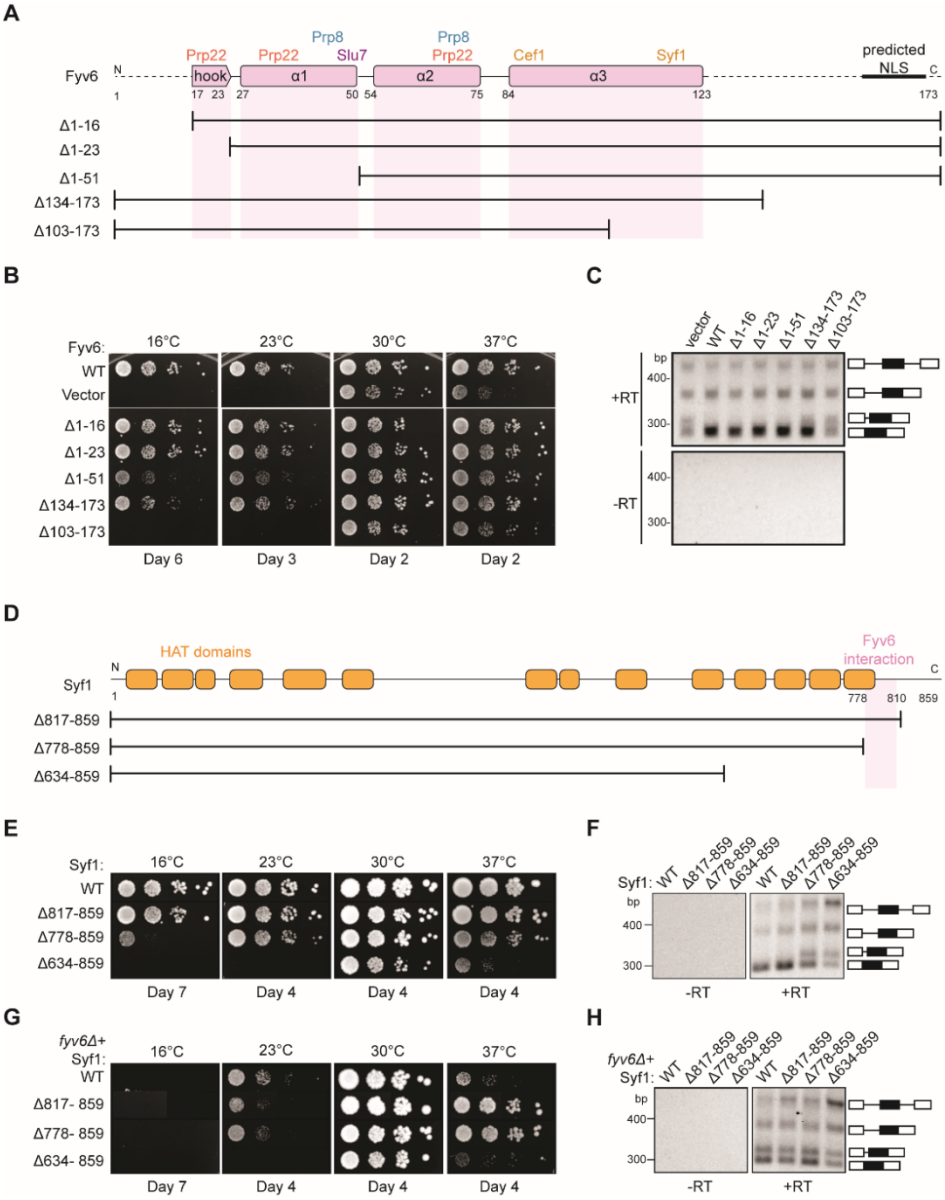

Figure 5. Structure-based analysis of Fyv6 domain function. A) Diagram of Fyv6 protein structure, protein interactors, and protein truncations. NLS= nuclear localization signal **B)** Spot dilution assay of strains with Fyv6 truncations on –Trp DO plates at different temperatures. Plates were imaged after the number of days indicated. **C)** Representative gel image of *SUS1* RT-PCR in strains with an empty vector or expressing the indicated Fyv6 variant. (+RT reactions contain reverse transcriptase; -RT control reactions do not contain reverse transcriptase.) **D)** Diagram of Syf1 protein structure and truncations. **E)** Spot dilution assay of strains with Syf1 truncations on –Trp DO plates at different temperatures. Plates were imaged after the number of days indicated. **F)** Representative gel image of *SUS1* RT-PCR in strains with an empty vector or expressing the indicated Syf1 variant. **G)** Temperature growth assay of strains with Syf1 truncations in a *fyv6Δ* background on YPD plates. Plates were imaged after the number of days indicated. **H)** Representative gel image of RT-PCR of *SUS1* in strains with plasmids containing WT Syf1 or a Syf1 truncation in a *fyv6Δ* background.

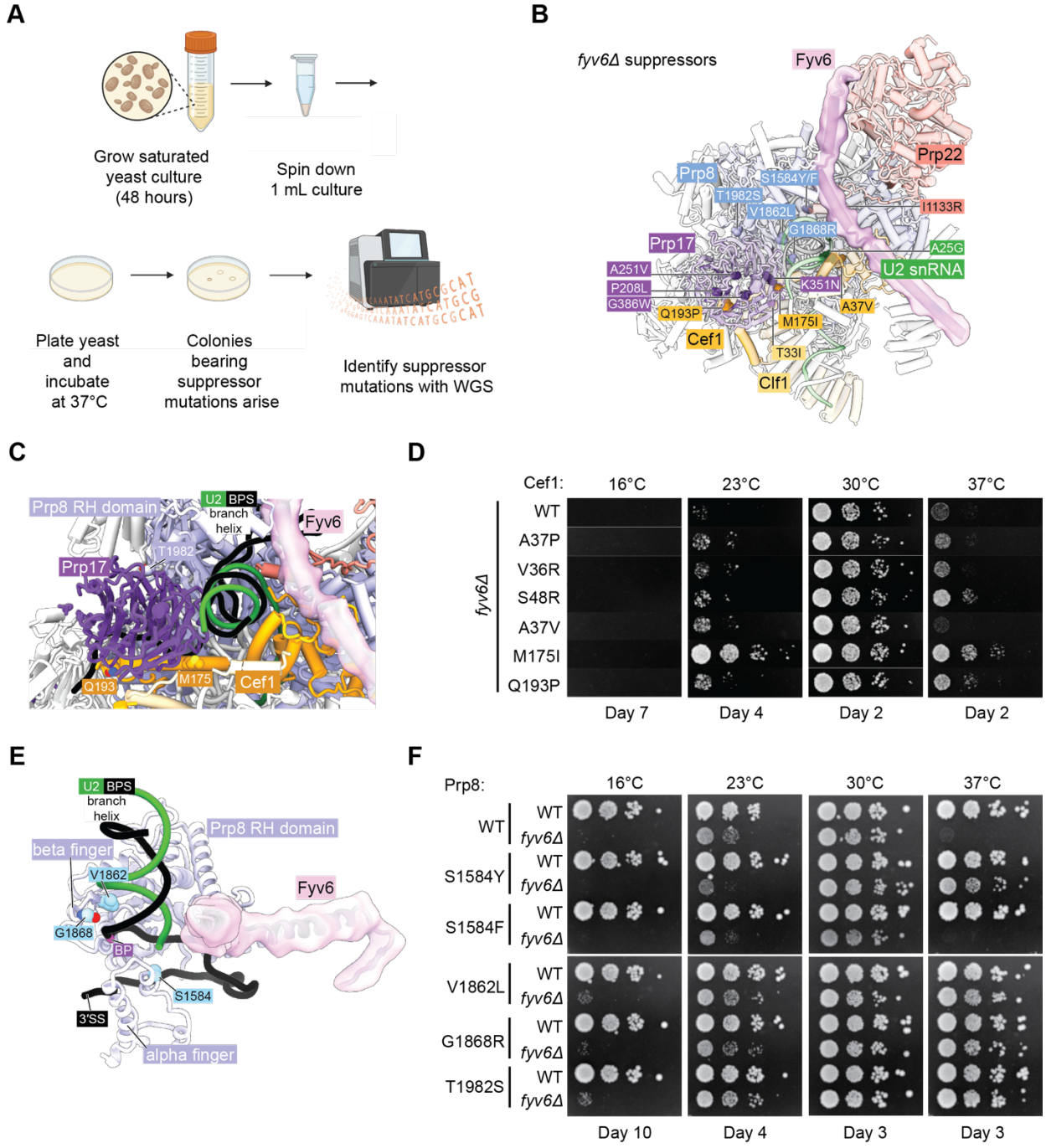

Figure 6. Identification of novel suppressors of *fyv6Δ* temperature sensitivity. A) Workflow for the suppressor screen. **B)** P complex spliceosome structure with *fyv6Δ* suppressor mutations labelled. (See **Supplemental Table S5**) **C)** Close-up view of Cef1 and Prp8 suppressor mutations in P complex. **D)** Spot dilution temperature growth assay with Cef1 mutants on YPD plates. Plates were imaged after the number of days indicated. **E)** Close-up view of Prp8 mutations in P complex. **F)** Spot dilution temperature growth assay with Prp8 mutants on YPD plates. Plates were imaged after the number of days indicated.

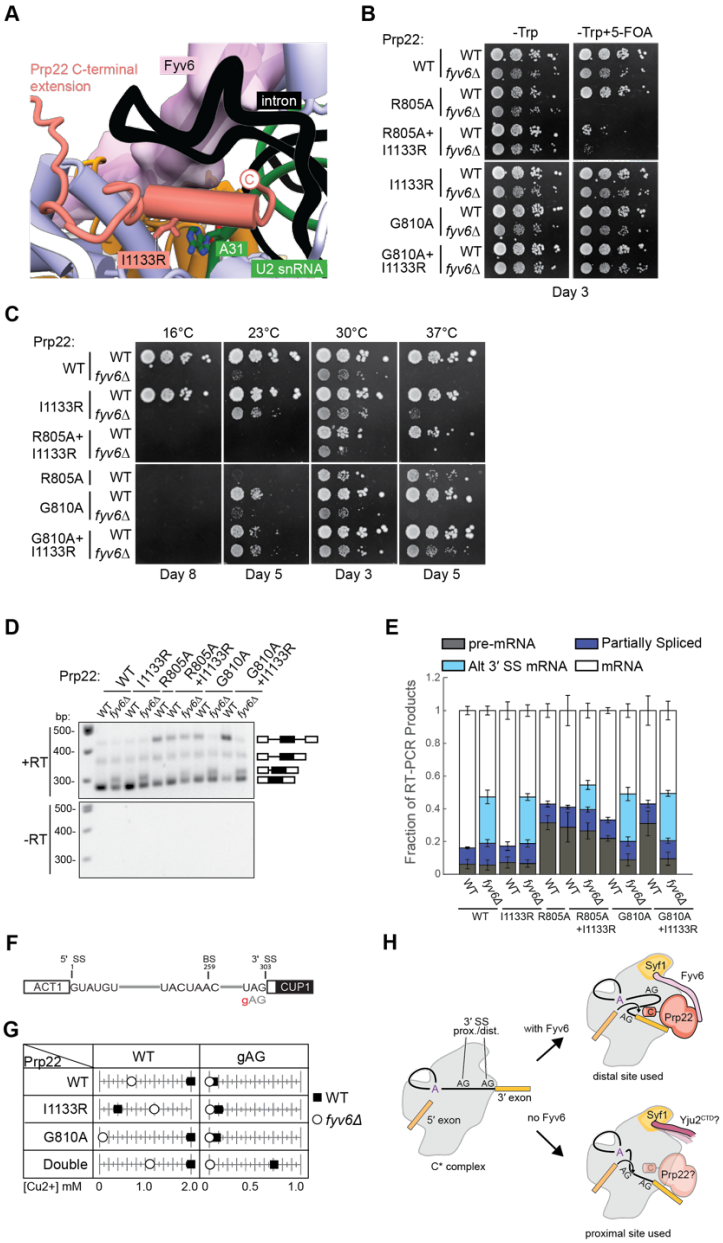

Figure 7. Genetic interactions between Prp22 and Fyv6. A) Location of the Prp22 I1133R *fyv6Δ* suppressor in the P complex structure. **B)** Spot dilution growth assay with Prp22 mutants in WT or *fyv6Δ* backgrounds grown on –Trp DO or –Trp+5-FOA plates. Plates were imaged after 3 days at 30°C. **C)** Spot dilution growth assay with strains containing Prp22 mutants on YPD plates at different temperatures. Plates were imaged after the number of days indicated. **D)** Representative gel of *SUS1* RT-PCR products in strains with Prp22 mutants in the presence or absence of Fyv6. **E)** Quantitation of band intensities for each *SUS1* splice isoform as a fraction of total product in the lane. Bars indicate average ± SD of *N*=3 replicates. **F)** ACT1-CUP1 reporter construct with the location of the 3' SS substitution noted. **G)** Copper tolerance for each ACT1-CUP1 reporter with each Prp22 allele in strains with (■) or without (○) Fyv6 present. Shown is a representative, single replicate of *N*=3. **H)** Model for the role of Fyv6 during the 2nd step. Fyv6 interacts with Syf1 and Prp22 and promotes usage of BP distal 3' SS. When Fyv6 is absent, BP proximal 3' SS are favored. It is possible that lack of Fyv6 also results in the presence of Yju2 during exon ligation and relaxing of the requirement for Prp22 at this step.